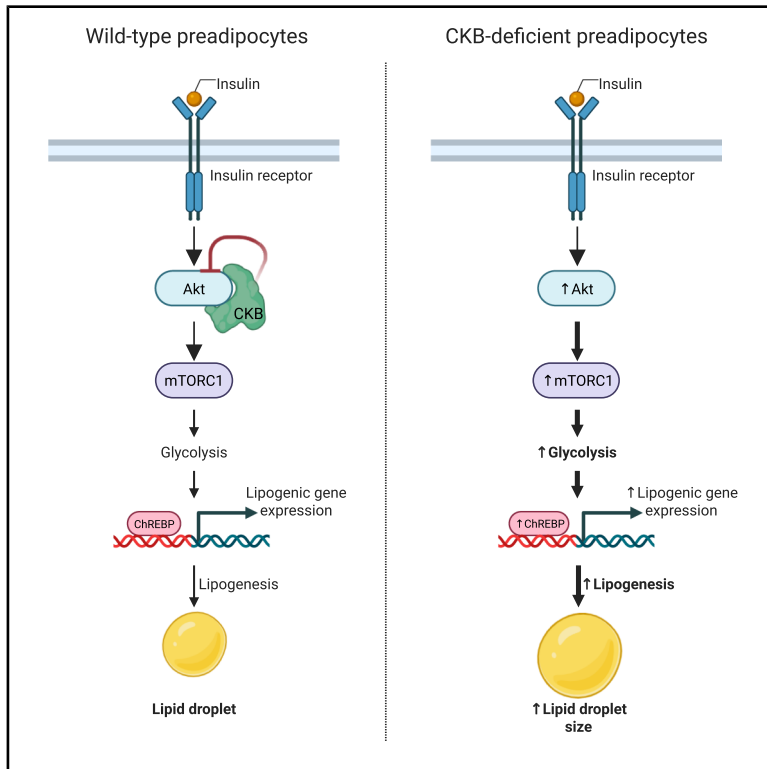


Creatine kinase B regulates glycolysis and *de novo* lipogenesis pathways to control lipid accumulation during adipogenesis

Graphical abstract



Authors

Gianluca Renzi, Romane Higos, Ivan Vlassakev, ..., Janane F. Rahbani, Simon Lecoutre, Salwan Maqdasy

Correspondence

simon.lecoutre@inserm.fr (S.L.),
salwan.maqdasy@ki.se (S.M.)

In brief

Renzi et al. identify creatine kinase B (CKB) as a metabolic sensor during white adipocyte differentiation. By modulating AKT, CKB fine-tunes insulin signaling and glycolysis to restrain ChREBP activation, thereby controlling *de novo* lipogenesis. This work links creatine metabolism to nutrient-responsive transcriptional regulation of lipid accumulation.

Highlights

- CKB and CKMT2 are progressively upregulated during white adipocyte differentiation
- Loss of CKB increases glycolytic flux, fueling glucose-driven lipid synthesis via ChREBP
- CKB fine-tunes AKT activity and modulates insulin-stimulated AKT-mTORC1 signaling



Report

Creatine kinase B regulates glycolysis and *de novo* lipogenesis pathways to control lipid accumulation during adipogenesis

Gianluca Renzi,¹ Romane Higos,^{1,2} Ivan Vlassakev,¹ Abdoul Akim Bello,³ Muhammad Omar-Hmeadi,⁴ Mattias Hansen,¹ Fatiha Merabtene,² Christine Rouault,² Ondrej Hodek,⁵ Lucas Massier,^{1,6} Bruno Antony,³ Geneviève Marcelin,² Janane F. Rahbani,⁷ Simon Lecoutre,^{2,9,*} and Salwan Maqdasy^{1,8,9,10,*}

¹Department of Medicine (H7), Karolinska Institutet, ME Endokrinologi, Karolinska University Hospital Huddinge, Huddinge 141 83, Sweden

²Nutrition and Obesity: Systemic Approaches Research Group (Nutri-Omics), Sorbonne Université, INSERM, Paris 75013, France

³Université Côte d'Azur, CNRS and Inserm, Institut de Pharmacologie Moléculaire et Cellulaire, UMR 7275, Sophia Antipolis, France

⁴Department of Animal Biosciences, Swedish University of Agricultural Sciences, Uppsala, Sweden

⁵Swedish Metabolomics Center, Department of Forest Genetics and Plant Physiology, Swedish University of Agricultural Sciences, Umeå, Sweden

⁶Helmholtz Institute for Metabolic, Obesity and Vascular Research (HI-MAG) of the Helmholtz Zentrum München at the University of Leipzig and University Hospital Leipzig, Leipzig, Germany

⁷Section of Hematology and Oncology, Department of Medicine, The University of Chicago, Chicago, IL 60637, USA

⁸ANOVA, Karolinska University Hospital, Stockholm, Sweden

⁹These authors contributed equally

¹⁰Lead contact

*Correspondence: simon.lecoutre@inserm.fr (S.L.), salwan.maqdasy@ki.se (S.M.)

<https://doi.org/10.1016/j.celrep.2025.116489>

SUMMARY

White adipocyte differentiation or adipogenesis requires coordination of metabolic sensing and transcriptional modifications to orchestrate lipid storage. Creatine and its kinases are implicated in adipose energy buffering, but the roles of cytosolic (CKB) and mitochondrial (CKMT2) creatine kinases in adipogenesis are unclear. We find that both CKB and CKMT2 are progressively upregulated during differentiation. Functional studies show that CKB restrains *de novo* lipogenesis (DNL) by limiting activation of carbohydrate-responsive element-binding protein (ChREBP), a key regulator of lipogenic genes. Mechanistically, CKB interacts with AKT and regulates its activation in response to insulin. Loss of CKB causes persistent AKT-mTORC1 signaling, increases glycolytic flux, and enhances ChREBP activation, thereby promoting glucose-derived lipid synthesis. Thus, CKB acts as a metabolic rheostat linking creatine-kinase activity to insulin signaling and nutrient-responsive transcription. We propose a CKB-AKT-ChREBP regulatory axis that contributes to metabolic remodeling and lipid homeostasis during adipocyte differentiation.

INTRODUCTION

Lipid turnover is essential for maintaining metabolic homeostasis, allowing white adipose tissue (WAT) to safely store excess nutrients during periods of energy surplus.¹ However, under chronic overnutrition, sustained lipid accumulation in WAT and the liver promotes lipotoxicity, driving insulin resistance and the development of type 2 diabetes (T2D).^{2,3} To mitigate this, lipid synthesis and storage are tightly regulated across tissues, with WAT and the liver serving as the primary lipogenic organs.⁴ WAT adapts by expanding through hypertrophy of existing adipocytes and through adipogenesis from resident precursors, processes essential for preserving adipose plasticity and mitigating ectopic lipid deposition.^{2,5–7} Disruption of these adaptive responses underlies the progression of cardiometabolic disease.^{5–8}

Adipogenesis is orchestrated by a well-defined transcriptional cascade involving the sequential activation of early (C/EBP β ,

C/EBP δ , glucocorticoid receptor, CREB) and late (C/EBP α , PPAR γ) regulators that establish and maintain adipocyte identity.^{7,9,10} While these transcriptional mechanisms are well characterized, the metabolic remodeling that fuels adipogenesis and supports lipid accumulation *in vivo* remains poorly understood. A central metabolic pathway in this process is *de novo* lipogenesis (DNL), which converts carbohydrate-derived acetyl-CoA into fatty acids.¹¹ In differentiating human adipocytes, DNL can supply the full complement of fatty acids required for maturation.¹² Indeed, fetal human adipocytes exhibit high lipogenic capacity as they develop into mature fat cells,¹³ and *in vitro*, human preadipocytes can fully differentiate and accumulate lipid droplets even in the absence of an exogenous fat source.¹⁴ Although the liver is the major site of systemic lipid synthesis, adipose DNL plays a distinct and protective role by channeling potentially toxic sugars into inert lipid stores, thereby buffering metabolic stress.¹¹



Paradoxically, DNL has shown tissue-specific associations with metabolic disease: it is positively correlated with insulin resistance in the liver but negatively correlated in adipose tissue.^{11,15,16} In both obese mice and individuals with obesity, DNL flux in WAT is often suppressed, suggesting a link to insulin sensitivity.¹⁷ Despite this clinical relevance, the molecular and metabolic mechanisms that regulate DNL during adipogenesis remain incompletely defined. Recent studies have suggested that amino acid metabolism may support lipid anabolism during adipocyte differentiation; however, whether additional energetic pathways contribute to this process is still unclear.^{18–20}

Using integrated transcriptomic and proteomic analyses, we identified significant changes in the creatine kinase system during adipogenesis. Creatine functions as a cellular energy buffer through the action of mitochondrial CKMT2 and cytosolic creatine kinase B (CKB), which shuttle high-energy phosphate groups between subcellular compartments.²¹ While prior studies have linked creatine and CKB to mitochondrial activity, thermogenesis, whole-body energy expenditure and inflammation,^{22–26} their role in white adipocyte differentiation and lipogenesis has remained undefined.

Here, we demonstrated that CKB acts as a metabolic gatekeeper of lipogenesis during adipogenesis. We found that CKB is as a key regulator of adipogenesis, insulin signaling, and fat storage via DNL. By fine-tuning insulin-mediated AKT pathway activation, CKB helps control the balance between anabolic signaling and lipid synthesis. Loss of CKB led to sustained AKT-mTORC1 activity, enhanced glycolysis, and increased carbohydrate-responsive element-binding protein (ChREBP)-driven transcription of lipogenic genes, thereby fueling DNL. These results reveal a novel CKB-AKT-ChREBP axis linking creatine metabolism to insulin-dependent lipogenesis. Together with recent studies on CKB's role in regulating fat cell bioenergetic and inflammatory status,^{22,23,26} our findings position CKB as a metabolic gatekeeper of adipose tissue function and systemic metabolism.

RESULTS

Temporal induction of creatine kinases reflects metabolic reprogramming during adipogenesis

To investigate metabolic reprogramming during human adipogenesis, we analyzed time-resolved transcriptomic data from the FANTOM5 consortium,²⁷ capturing the differentiation of our *in vitro* differentiating human preadipocytes from day 0 (D0) to fully mature adipocytes at D12. At each time point, we identified significantly enriched pathways and visualized them as an interconnected network of metabolic processes. This revealed extensive remodeling of cellular metabolism at the end of differentiation (Figure 1A), with amino acid-related pathways being particularly enriched. Among these, the arginine-proline metabolism pathway displayed one of the strongest inductions in expression throughout adipogenesis (Figure S1A). This finding aligns with emerging research highlighting amino acid metabolism as a critical regulator in adipocyte differentiation and function.^{18,19,28–30} Within this pathway, *CKB* and *CKMT2*, encoding cytosolic and mitochondrial creatine kinases, respectively, stood out among the most upregulated genes throughout adipogenesis

(Figures 1B and S1B). Both western blotting and LC-MS-based proteomics^{31,32} demonstrated a sustained increase in CKB and CKMT2 expression at the protein level across the course of differentiation (Figures 1C and 1D).

Notably, the expression of both cytosolic CKB and mitochondrial CKMT2 was markedly upregulated only during the late phase of adipocyte differentiation, becoming prominent after D5 (Figure 1D). Prior studies have established that triiodothyronine (T_3) enhances creatine kinase expression and activity in high-energy-demand tissues such as cardiac and skeletal muscle.³⁴ Given that T_3 is a component of the adipogenic differentiation cocktail used in human preadipocyte cultures, we investigated whether thyroid hormone directly contributes to creatine kinase regulation during adipogenesis. Individual components of the differentiation cocktail were sequentially omitted between D5 and D8. While removal of the PPAR γ agonist had no discernible effect, the omission of T_3 revealed a specific requirement for thyroid hormone in driving creatine kinase expression (Figure S1C). To directly assess responsiveness to thyroid hormone, differentiating adipocytes were deprived of the full differentiation cocktail from D5 to D8 and subsequently acutely stimulated with T_3 . This brief exposure was sufficient to robustly induce *CKB* and *CKMT2* mRNA expression (Figure 1E). Notably, this induction coincided with enrichment of thyroid hormone signaling signatures, consistent with the inclusion of T_3 as a key component of the adipogenic cocktail. In line with these observations, motif enrichment analysis identified multiple thyroid hormone receptor (THR) binding sites within regulatory regions proximal to the *CKB* and *CKMT2* loci (Figure S1D).

Our *in vitro* findings were corroborated by spatial transcriptomic profiling of human WAT,^{32,33} which showed that *CKB* and *CKMT2* expression is predominantly enriched in mature adipocytes, with fewer expression in preadipocytes (Figure 1F). Further validation using qPCR on isolated cells from human subcutaneous WAT biopsies confirmed significantly higher expression of *CKB* and *CKMT2* in mature adipocytes compared to preadipocytes (Figure 1G). In summary, these findings identify CKB and CKMT2 as key T_3 -responsive metabolic genes that are robustly induced during human adipogenesis.

Silencing of CKB enhances triglyceride accumulation via DNL without altering adipogenesis

To determine the functional role of creatine kinase activity during human adipogenesis, we selectively silenced *CKB* and *CKMT2* in primary human preadipocytes using lipid nanoparticle-delivered small interfering RNAs (siC, siCKB, and siCKMT2). This approach achieved robust knockdown of both mRNA and protein levels throughout the differentiation process (Figures 2A and 2B). Surprisingly, loss of either CKB or CKMT2 did not impair adipocyte differentiation, as the expression of key adipogenic markers, including ADIPOQ (adiponectin) and PPAR γ , remained unchanged at both mRNA and protein levels (Figures 2B and S2A–S2C). However, CKB depletion markedly increased intracellular lipid accumulation, as shown by enhanced BODIPY intensity and lipid droplet area per adipocyte. This was accompanied by excessive triglyceride (TG) accumulation in siCKB cells, whereas CKMT2 knockdown had no such effect (Figures 2C and 2D). This suggests a selective role for cytosolic creatine kinase in

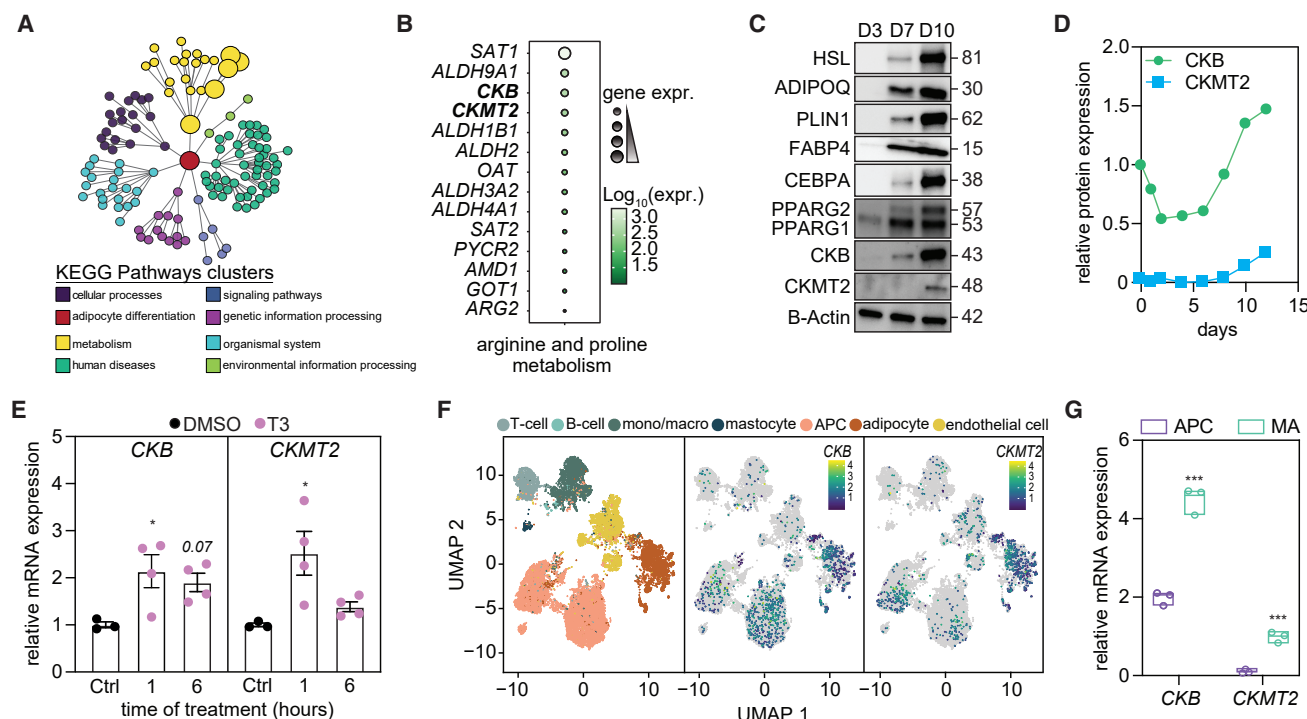


Figure 1. Temporal induction of creatine kinases reflects metabolic reprogramming during adipogenesis

(A) KEGG enrichment analysis of all significantly enriched pathways at day 12 (D12) of *in vitro* human white preadipocyte differentiation (FANTOM5 dataset),²⁷ with pathways clustered into functional superfamilies. Color-coding legend is shown below the plot.

(B) Gene expression ranking of all the genes upregulated in “arginine and proline metabolism” KEGG pathway at D12 of differentiation. Gene name is specified on the left. Size and color of the dots are related to gene expression.

(C) Representative immunoblot of differentiating *in vitro* human white preadipocytes at D3, D7, and D10 of differentiation, demonstrating progressive upregulation of creatine kinases and adipogenic markers during adipogenesis.

(D) Proteomics analysis of differentiating human white preadipocytes from D0 (start of differentiation) to D12, showing temporal expression patterns of CKB and CKMT2.³¹ Values are mean expressions for each time point.

(E) Relative mRNA expression of CKB and CKMT2 in cells cultured without adipogenic cocktail from D5 to D8, followed by acute stimulation with triiodothyronine (T3) for 1 or 6 h. Data are presented as mean \pm SEM. Statistical significance was determined using one-way ANOVA followed by Dunnett’s multiple-comparison test. * $p < 0.05$ vs. control (DMSO, no T3 treatment).

(F) UMAPs plots of human white adipose tissue single-nucleus transcriptomes; on the left, representation of each cell type in relation to clusters (color coded, legend above the plot); on the center and left, expression of CKB and CKMT2, respectively.^{32,33}

(G) Relative mRNA expression of CKB and CKMT2 in white adipose tissue fractions isolated from human biopsies—adipose precursor cells (APCs) and mature adipocytes (MAs). Values are presented as min-max. p value was calculated by Student’s t -test. *** $p < 0.001$.

limiting lipid storage capacity. The link between CKB and lipid accumulation was corroborated in human adipose tissue, where CKB (but not CKMT2) mRNA levels negatively correlated with adipocyte cell volume, even after adjusting for body mass index (BMI; Figure 2E).

To explore the molecular mechanisms underpinning this phenotype, we performed RNA-seq on siCKB, siCKMT2, and control adipocytes. Principal component analysis (PCA) revealed distinct transcriptional signatures for each condition (Figure S2D), and knockdown efficiency was confirmed (Figure S2E). While adipogenic gene networks remained largely intact, siCKB but not siCKMT2 cells exhibited marked upregulation of DNL-associated pathways (Figures 2F and S2F). Indeed, the expression of genes encoding key DNL enzymes was increased only in siCKB cells compared to both controls and siCKMT2 (Figure 2G). This transcriptional reprogramming translated into functional changes in lipid metabolism. Using

in vitro DNL assays with [^3H]-glucose incorporation into TG, we observed a marked increase in insulin-stimulated lipogenesis in siCKB cells (Figure 2H). Consistently, intracellular palmitate levels, one of the major products of DNL, were elevated in siCKB cells (Figure 2I), establishing a link between CKB suppression and enhanced TG accumulation through DNL.

To further test this relationship, we overexpressed CKB (CKB^{oe}) using a dCas9-VPR activation system prior to induction of adipogenesis. While CKB^{oe} did not alter adipogenic markers (Figure 2J), it suppressed DNL gene expression and significantly reduced lipid accumulation in mature adipocytes (Figures 2K, 2L, and S2G).

To explore the *in vivo* relevance of these findings, we analyzed adipocyte-specific Ckb knockout mice (Ckb^{AdipoCre})²² and challenged them with a high-fat diet (HFD) for 6 weeks. These mice exhibited marked induction in the expression of DNL-associated genes in inguinal WAT with preserved expression of mature

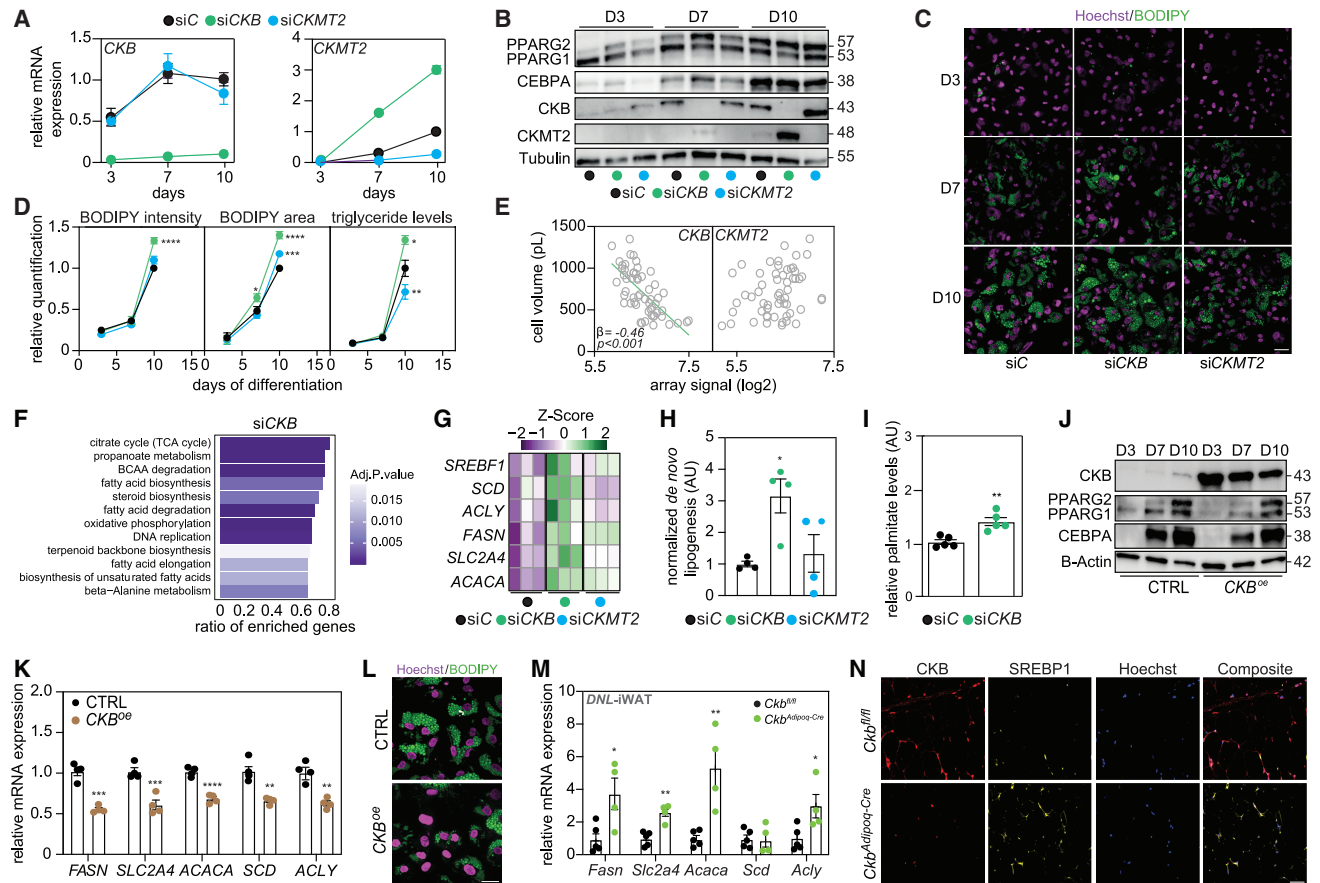


Figure 2. Silencing of creatine kinase B enhances triglyceride accumulation via *de novo* lipogenesis without altering adipogenesis

(A) Relative mRNA expression of CKB and CKMT2 in differentiating human white preadipocytes transfected at day -1 (D-1; 24 h before induction of differentiation) with non-silencing control (siC), CKB-targeting (siCKB), or CKMT2-targeting (siCKMT2) siRNA. Cells were collected at D3, D7, and D10 of differentiation for analysis. Data are presented as mean \pm SEM.

(B) Representative immunoblot of differentiating *in vitro* human white preadipocytes transfected with siC, siCKB, or siCKMT2 at D-1. Cells were lysed at D3, D7, and D10 for analyses.

(C) Representative immunohistochemical staining for Hoechst (nuclei) and BODIPY (lipid droplets) in human white preadipocytes transfected with siC, siCKB, or siCKMT2 24 h before induction of differentiation (D-1). Cells were fixed for staining at D3, D7, and D10 of differentiation. Scale bar represents 20 μ m.

(D) Quantification of BODIPY intensity per cell on the left, BODIPY area per cell on the center, and triglycerides content (measured by triglyceride quantification kit) on the right. siC-, siCKB-, and siCKMT2-transfected cells were analyzed at D3, D7, and D10 of differentiation. BODIPY values were normalized to Hoechst signal; triglycerides were normalized to total protein content. Values are mean \pm SEM. p value was calculated by two-way ANOVA and Tukey's multiple-comparison test, $n > 10$, * $p < 0.05$, ** $p < 0.01$, *** $p < 0.001$, **** $p < 0.0001$.

(E) Correlation between CKB (left) or CKMT2 (right) mRNA expression and cell volume in human subcutaneous white adipose tissue from subjects with obesity (OB, $n = 30$) or without obesity (NO, $n = 26$).^{26,35} Statistical significance was determined by Spearman correlation; standardized β values were calculated with p values adjusted for body mass index (BMI).

(F) KEGG pathways enriched in siCKB cells compared to siC; color represents significance of enrichment, and on the x axis is displayed the enrichment ratio of genes/tot gene ontologies.

(G) Heatmap representing the expression of genes involved for *de novo* lipogenesis (DNL) in cells transfected with siC, siCKB, or siCKMT2 at D-1 and lysed for analyses at D10 of differentiation. Values are row centered and scaled.

(H) Stimulated DNL in human white preadipocytes transfected at D-1 with siC, siCKB, or siCKMT2 and harvested at D10 of differentiation. Values were normalized to total protein content and are presented as mean \pm SEM. Statistical significance was assessed by one-way ANOVA with Dunnett's multiple-comparison test vs. siC. * $p < 0.05$.

(I) Targeted metabolomic level of intracellular palmitate in human white preadipocytes transfected with siC or siCKB at D-1 and lysed for analyses at D10 of differentiation. Values are mean \pm SEM. p value was calculated by Student's t -test, ** $p < 0.01$.

(J) Representative immunoblot of differentiating human white preadipocytes transfected at D-1 with mRNA encoding catalytically inactive Cas9 coupled to a VPR complex with or without guide RNAs (gRNAs) targeting the CKB promoter, harvested at D3, D7, and D10 of differentiation.

(K) Relative mRNA expression of DNL-related genes of differentiating human white preadipocytes transfected with mRNA encoding catalytically inactive Cas9 coupled to a VPR complex with or without guide RNA targeting CKB promoter and harvested at D10 of differentiation. Values are mean \pm SEM. p value was calculated by Student's t test, ** $p < 0.01$, *** $p < 0.001$, **** $p < 0.0001$.

(legend continued on next page)

adipocyte markers (Figures 2M and S2H), while this effect was absent in the epididymal depot (Figure S2I). Immunofluorescence analysis revealed elevated levels of SREBP1, one of DNL markers, supporting CKB's repressive role *in vivo* (Figures 2N and S2J).

To independently validate the link between CKB and DNL, we employed multiple complementary strategies. First, to pinpoint the critical window of CKB's influence on DNL, we temporally knocked down *CKB* at D3 and D8 of differentiation. Early knockdown (D3) recapitulated the effects on DNL gene induction (Figure S2K), whereas late knockdown (D8) failed to induce DNL genes (Figure S2L), suggesting a temporal window during early differentiation where CKB modulates lipogenesis. Second, *CKB* knockdown replicated the pro-lipogenic phenotype across distinct preadipocyte models, including female-donor-derived human white preadipocytes, human adipose-derived stem (hMADS) cells,³⁶ and primary murine preadipocytes isolated from inguinal WAT of female mice, demonstrating conserved regulation of DNL (Figures S2M–S2O). Finally, CRISPR-Cas9-mediated *CKB* knockout in *in vitro* human white preadipocytes recapitulated the phenotype, excluding potential off-target effects of siRNA-based silencing (Figure S2P).

Collectively, these findings position the cytosolic CKB as a regulator of adipocyte lipid storage and a molecular fine-tuner on DNL during human adipogenesis.

CKB depletion drives ChREBP-mediated lipogenesis through enhanced glycolytic flux

Given that glucose is the primary carbon source for DNL,¹¹ we first assessed glucose uptake in adipocytes lacking CKB. The expression of *SLC2A4*, which encodes the insulin-responsive glucose transporter *GLUT4*, was significantly increased in siCKB adipocytes (Figure 2G), indicating enhanced glucose influx in the absence of CKB. Based on this observation, and on prior evidence linking glycolysis to lipogenesis,^{11,37} we hypothesized that *CKB* depletion promotes glycolytic flux, thereby fueling DNL. To test this, we measured glycolytic activity on D10 of differentiation using Seahorse extracellular flux analysis. siCKB adipocytes exhibited a pronounced increase in extracellular acidification rate (ECAR; Figure 3A), consistent with elevated glycolytic throughput. Concurrently, intracellular ATP levels were significantly elevated (Figure S3A), while oxygen consumption rate (OCR) remained unchanged (Figure S3B), suggesting that metabolic reprogramming was specific to glycolysis rather than mitochondrial oxidative phosphorylation. To evaluate whether this increase in glycolysis supplies precursors for lipogenesis, we performed targeted metabolomic profiling. This revealed substantial accumulation of glycolysis-related intermediates, including fructose-6-phosphate (F6P), xylulose-5-phosphate (X5P), pyruvate, and lactate (Figure 3B), which can contribute to fatty acid synthesis.³⁸ We also observed

elevated succinate levels, a tricarboxylic acid (TCA) cycle intermediate that could support lipogenesis through citrate production¹⁷ (Figure S3C).

The elevation of X5P in siCKB adipocytes prompted us to examine the activation of ChREBP, a central transcriptional regulator of DNL that is thought to be stimulated by glycolysis-derived sugar phosphates such as X5P.³⁸ ChREBP, encoded by the *MLXIPL* gene, exists as a glucose-sensitive full-length isoform (~100 kDa) with modest activity, and a shorter, transcriptionally potent isoform (~35 kDa) induced by glycolytic flux.^{39–41} Lacking the N-terminal low-glucose inhibitory domain (LID), the truncated isoform localizes constitutively to the nucleus and is ~20-fold more active. Together, these isoforms create a feedforward circuit in which elevated glucose promotes its own conversion into lipids.^{39–41} Strikingly, siCKB adipocytes showed a sharp rise in the active 35 kDa ChREBP isoform (Figures 3C and S3D). To functionally test the requirement for ChREBP in mediating this phenotype, we silenced *MLXIPL* in siCKB adipocytes at D8 of differentiation. *MLXIPL* knockdown efficiently suppressed ChREBP protein expression (Figure 3D) and completely abrogated the induction of DNL target genes and lipid accumulation observed in *CKB*-deficient cells (Figures 3E and 3F). These findings support a model in which ChREBP acts as a downstream effector of *CKB* loss, linking enhanced glycolytic flux and sugar phosphate accumulation to the transcriptional activation of lipogenesis.

To directly test whether glycolytic flux is the upstream driver of ChREBP activation and lipogenesis in *CKB*-deficient adipocytes, we treated siCKB cells with 2-deoxy-D-glucose (2-DG), a competitive inhibitor of glycolysis.⁴² As expected, 2-DG treatment normalized glucose uptake in siCKB adipocytes to levels observed in control cells (Figure 3G) and fully reversed the metabolic reprogramming induced by *CKB* loss. Specifically, 2-DG abrogated ChREBP protein accumulation, suppressed the expression of ChREBP target genes involved in DNL, and reduced BODIPY intensity per adipocyte (Figures 3H–3J). These results confirm that increased glycolytic flux is required for ChREBP activation and lipogenesis in the absence of *CKB*. Collectively, our findings define the *CKB*-glycolysis-ChREBP regulatory axis, which governs lipid biosynthesis in human adipocytes.

CKB depletion is linked to elevated mTORC1 signaling

We next investigated the upstream mechanism by which *CKB* restrains glycolytic flux. We first evaluated the canonical creatine (Cr)-phosphocreatine (PCr) shuttle. Consistent with impaired cytosolic *CKB* activity, siCKB adipocytes exhibited a significant increase in the PCr-to-Cr ratio (Figure S4A), indicative of disrupted PCr cycling. However, supplementation with exogenous PCr (1–30 mM) during differentiation reduced *SLC2A4* mRNA expression encoding for *GLUT4* but failed to alter the classical

(L) Representative images of differentiating human white preadipocytes transfected with mRNA encoding catalytically inactive Cas9 coupled to a VPR complex cells with or without *CKB*-targeting guide RNAs fixed and stained at D10 of differentiation. Scale bar represents 10 μ m.

(M) Relative mRNA expression of DNL-related genes in inguinal white adipose tissue (iWAT) of *Ckb^{fl/fl}* and *Ckb^{Adipoq-Cre}* male mice. Values are mean \pm SEM. *p* value was calculated by Student's *t* test **p* < 0.05, ***p* < 0.01.

(N) Representative immunofluorescent staining of CKB, SREBP1, and Hoechst in paraffin-embedded inguinal WAT (iWAT) from *Ckb^{fl/fl}* and *Ckb^{Adipoq-Cre}* male mice. Group is specified on the left of the images and channel on top of them. Scale bar represents 50 μ m.

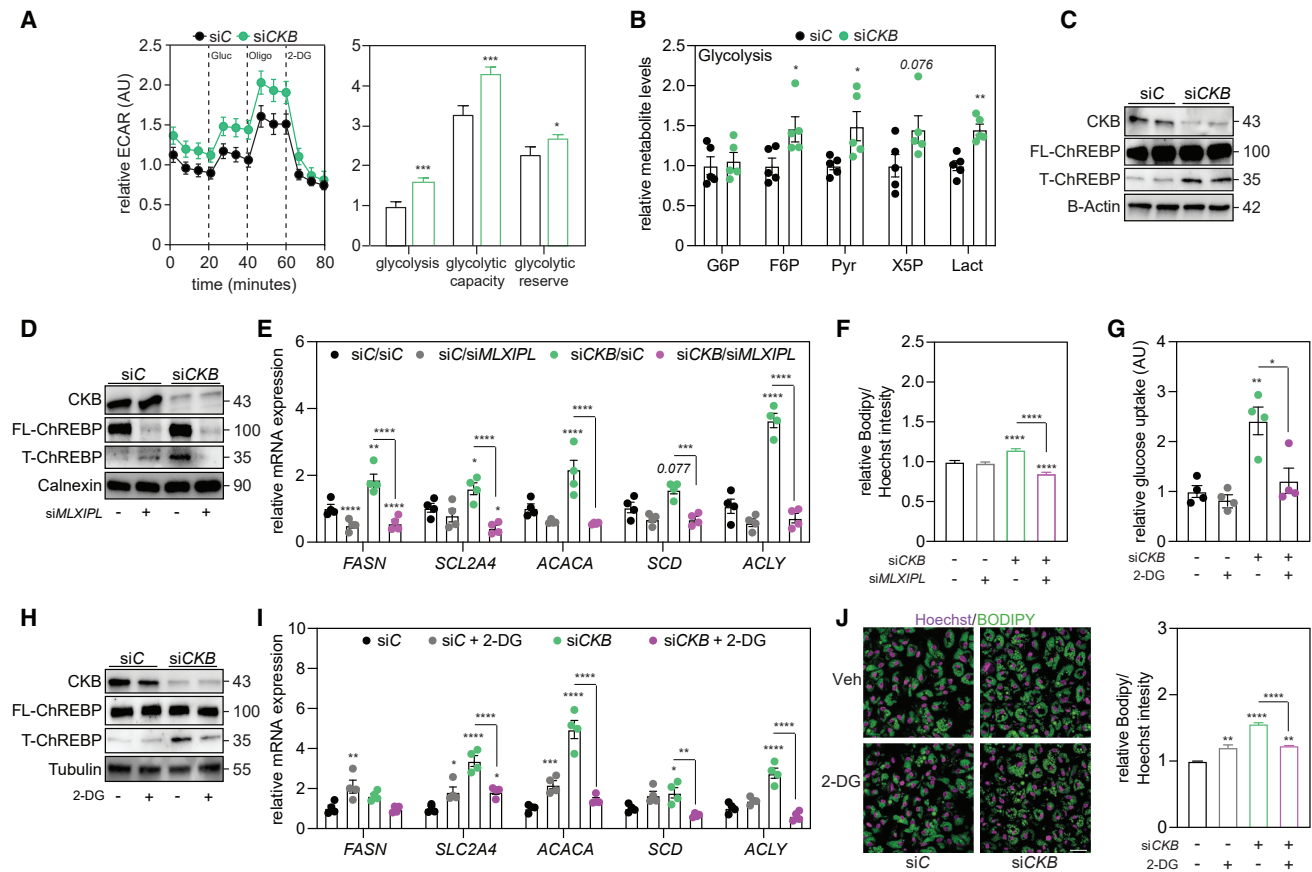


Figure 3. CKB depletion stimulates ChREBP-mediated lipogenesis through enhanced glycolytic flux

(A) On the left: representative Seahorse GlycoStress test analysis of extracellular acidification rate (ECAR) in human preadipocytes transfected at D-1 with siC or siCKB and analyzed after 10 days of differentiation. On the right: ECAR profile over time. Right: quantification of relative glycolysis, glycolytic capacity, and glycolytic reserve. Data are mean \pm SEM. Statistical significance was determined by Student's *t* test. $n > 10$, $*p < 0.05$, $***p < 0.001$. Abbreviations: Gluc, glucose; Oligo, oligomycin; 2-DG, 2-deoxy-glucose.

(B) Targeted metabolite levels related to glycolysis in *in vitro* human white preadipocytes transfected at D-1 with siC or siCKB and harvested at D10 of differentiation for analysis. Data are presented as mean \pm SEM. *p* value was calculated using Student's *t* test. $*p < 0.05$, $**p < 0.01$. Abbreviations: G6P, glucose-6-phosphate; F6P, fructose-6-phosphate; X5P, xylulose-5-phosphate; Pyr, pyruvate; Lact, lactate.

(C) Representative immunoblot of ChREBP isoforms in human preadipocytes transfected at D-1 with control siC or siCKB and harvested at D10 of differentiation. Bands correspond to the full-length (FL) and the truncated, transcriptionally active (T) of ChREBP.

(D) Representative immunoblot of cells transfected at D-1 with siC or siCKB and re-transfected at D8 with siC or siMLXIPL (targeting ChREBP expression), confirming ChREBP knockdown at D10 of differentiation. Bands correspond to full-length (FL) and truncated, transcriptionally active (T) isoforms of ChREBP.

(E) Relative mRNA expression of DNL-related genes in early siC- and siCKB-transfected cells (transfection at D-1), re-transfected at D8 with siC or siMLXIPL, and harvested for analysis at D10 of differentiation. Values are mean \pm SEM. *p* value was calculated with two-way ANOVA and Tukey's multiple-comparison test, comparing all conditions to siC unless indicated otherwise, $*p < 0.05$, $**p < 0.01$, $***p < 0.001$, $****p < 0.0001$.

(F) Representative high-throughput quantification of BODIPY staining in early siC- or siCKB-transfected cells (transfected at D-1) re-transfected at D8 with siC or siMLXIPL, and harvested for analysis at D10 of differentiation. BODIPY intensity was normalized to Hoechst signal. Data are mean \pm SEM. Statistical significance was determined by two-way ANOVA with Tukey's multiple-comparison test, comparing all conditions to siC unless indicated otherwise. $n > 10$, $****p < 0.0001$.

(G) Representative glucose uptake assay using 2-deoxy-D-[1- 3 H]-glucose in human preadipocytes transfected on D-1 with siC or siCKB. At D10 of differentiation, cells were treated with vehicle or 2-DG for 48 h and then harvested for analysis. Data are presented as mean \pm SEM. *p* value was calculated using two-way ANOVA and Tukey's multiple-comparison test, comparing all conditions to siC unless indicated otherwise, $*p < 0.05$, $**p < 0.01$.

(H) Representative immunoblot showing ChREBP protein isoforms in cells transfected on D-1 with siC or siCKB. At D10 of differentiation, cells were treated with vehicle or 2-DG for 48 h and then harvested for analysis.

(I) Relative mRNA expression of DNL-related genes in differentiating human white preadipocytes transfected at D-1 with siC or siCKB, treated D10 of differentiation with vehicle or 2-DG for 48 h, and then harvested for analysis. Data are presented as mean \pm SEM. *p* value was calculated using two-way ANOVA and Tukey's multiple-comparison test, comparing all conditions to siC unless indicated otherwise, $*p < 0.05$, $**p < 0.01$, $***p < 0.001$, $****p < 0.0001$.

(J) On the left, representative immunohistochemical of nuclei (Hoechst) and lipid droplets (BODIPY) in cells transfected at D-1 with siC or siCKB, incubated with vehicle or 2-DG for 48 h at D10 of differentiation, and fixed for analysis. Scale bar represents 20 μ m. Right: high-throughput quantification of BODIPY intensity normalized to Hoechst signal. Data are mean \pm SEM. Statistical significance was assessed by two-way ANOVA with Tukey's multiple-comparison test, comparing all conditions to siC unless indicated otherwise. $n > 10$ per group, $**p < 0.01$, $****p < 0.0001$.

DNL-related gene expression (Figure S4B), effectively excluding a PCR-mediated mechanism.

We next considered AMP-activated protein kinase (AMPK), a master energy sensor regulated by intracellular ATP levels and creatine metabolism,^{26,43} and a well-established suppressor of DNL.⁴⁴ In line with the observed increase in ATP levels (Figure S3A), CKB-depleted adipocytes exhibited reduced AMPK activity (based on phosphorylation of threonine 172; Figures 4A and S4C). However, pharmacological activation of AMPK using PF-739 induced AMPK phosphorylation but failed to totally reverse DNL-related gene expression in siCKB cells (Figures 4A and 4B).

Given prior evidence that creatine metabolism modulates mTORC1 signaling in other cell types,⁴⁵ we next investigated whether mTORC1 drives the ChREBP-dependent DNL observed upon CKB knockdown during human adipogenesis. Indeed, mTORC1 is a central nutrient- and energy-sensing kinase complex known to orchestrate anabolic programs such as glycolysis and lipogenesis.⁴⁶ CKB knockdown led to increased phosphorylation of P70S6K, a downstream target of mTORC1, indicative of enhanced mTORC1 activity (Figures 4C and S4C). To determine the functional relevance of this pathway, we treated siCKB adipocytes with rapamycin, a selective mTORC1 inhibitor.^{47,48} Rapamycin treatment markedly reduced P70S6K phosphorylation, DNL-related gene expression, and lipid accumulation in siCKB cells compared to controls (Figures 4C–4E), establishing mTORC1 as a key mediator of the metabolic and lipogenic effects observed upon CKB depletion. Importantly, this regulatory role is independent of CKB's canonical function within the PCr energy shuttle, revealing a non-canonical mechanism by which CKB modulates energy sensing and lipid metabolism in adipocytes.

CKB regulates DNL via AKT fine-tuning

We next investigated the upstream mechanism by which CKB controls mTORC1 activation in adipocytes. We first assessed the potential role of branched-chain amino acids (BCAAs), known activators of mTORC1.⁴⁹ However, varying extracellular BCAA concentrations across a physiological range during human adipogenesis had no effect on mTORC1 activity nor on DNL gene expression in siCKB adipocytes (Figures S4D and S4E), indicating that CKB regulates mTORC1 independently of BCAA signaling.

We then turned to the PI3K-AKT pathway, a central upstream regulator of mTORC1 and a key mediator of insulin-stimulated glucose metabolism in adipocytes.⁵⁰ AKT is not only a well-established activator of mTORC1 but also listed as a potential CKB interactor in the NCBI Gene database. Notably, previous studies have demonstrated CKB-AKT co-immunoprecipitation in both neuronal and cancer cell contexts,^{51,52} providing strong rationale for investigating this interaction in adipocytes. Immunoprecipitation of AKT in our human adipocyte model confirmed a physical association with CKB (Figure 4F), supporting the relevance of this interaction in the context of adipogenesis. Furthermore, CKB knockdown markedly increased AKT phosphorylation (Figure S4F), a reliable marker for the AKT protein kinase activity. To determine whether AKT activity is required for the lipogenic phenotype observed upon CKB depletion,

we treated siCKB adipocytes with MK-2206, a selective allosteric AKT inhibitor.⁵³ As a parallel control, we deprived adipocytes from insulin to inhibit AKT activation.⁵⁴ Interestingly, AKT-mTORC1-ChREBP activation is lost in siCKB cells in the absence of insulin (Figure 4G). Moreover, MK-2206 treatment fully abrogated the increase in P70S6K phosphorylation and ChREBP protein accumulation and significantly suppressed DNL-related gene expression, DNL process, and lipid accumulation in siCKB cells (Figures 4G–4J). These findings establish AKT as a key mediator of the metabolic reprogramming observed upon CKB depletion. Supporting this, insulin starvation and re-stimulation experiments showed that DNL-related gene overexpression in siCKB cells was normalized under insulin deprivation and fully restored following insulin reintroduction (Figure S4G), confirming that the lipogenic response is insulin dependent.

To confirm the specificity of this pathway, we re-expressed CKB at D8 in siC and siCKB adipocytes. CKB re-expression was confirmed at both the mRNA and protein levels (Figures 4K and S4H) and functionally reversed the elevated AKT phosphorylation and ChREBP protein accumulation (Figure 4K). This intervention fully rescued the lipogenic phenotype (Figures 4L and 4M), conclusively identifying CKB as a gatekeeper of TG accumulation during human adipogenesis. Finally, time-course analysis during differentiation revealed that CKB depletion initiates a cascade beginning with AKT phosphorylation, followed by enhanced glycolytic activity (measured by ECAR) and increased lactate production (Figures S4I–S4K).

Together, these findings establish CKB as an important regulator that sequesters AKT to limit insulin signaling and temper DNL via AKT-mTORC1-ChREBP.

DISCUSSION

WAT acts as a dynamic metabolic organ that governs energy storage and mobilization in response to nutrient availability.² Processes such as adipocyte differentiation, WAT expansion, and fat storage are tightly linked to metabolic sequelae.^{6,55} However, the precise molecular mechanisms that connect nutrient sensing to metabolic reprogramming, particularly the transcriptional control of lipid accumulation during adipogenesis, remain incompletely defined. Adipogenesis involves a coordinated series of transcriptional and metabolic events that enable preadipocytes to acquire the capacity to store TGs, a critical adaptation that buffers excess energy and preserves systemic metabolic homeostasis.^{2,5,6,56} Optimized lipid storage not only prevents lipotoxicity but also supports metabolically healthy WAT expansion.^{2,5,6} Although DNL contributes modestly to TG stores in mature adipocytes *in vivo*, it plays an essential role during differentiation by facilitating adipocyte maturation, enhancing lipid-buffering capacity, and promoting insulin sensitivity.^{12,17,37,57} Conversely, in hepatocytes, DNL drives metabolic dysfunction-associated steatotic liver disease.¹⁵ The contribution of creatine kinases to these processes has been poorly characterized, though creatine supplementation has been shown to mitigate hepatic steatosis in rodent models,^{58,59} suggesting a possible metabolic link between creatine metabolism and lipogenesis.

Here, we identify CKB as a non-canonical regulator of lipogenesis during adipogenesis. CKB expression increases

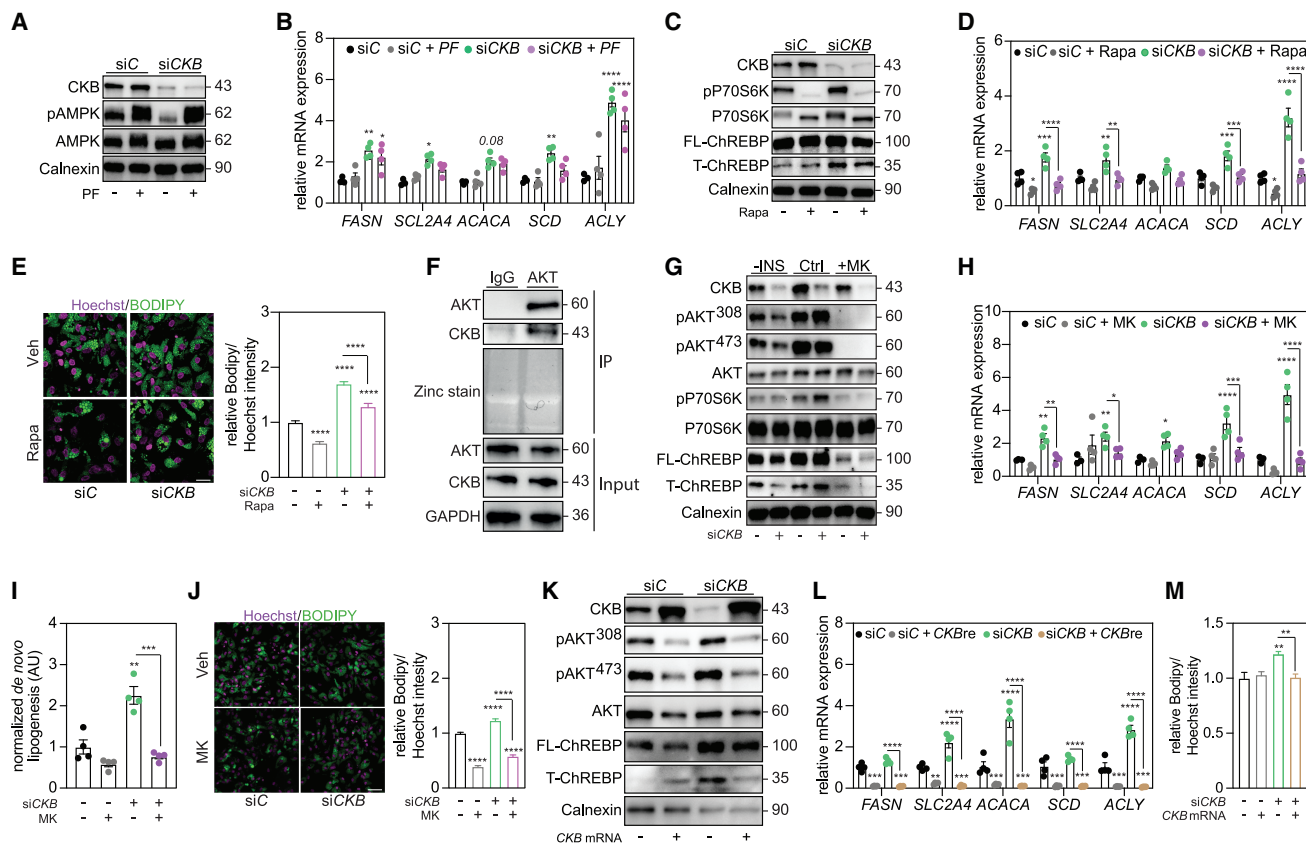


Figure 4. CKB modulates DNL by regulating AKT phosphorylation

(A) Representative immunoblot of cells transfected at D-1 with siC or siCKB. At D10 of differentiation, cells were treated with vehicle or PF-739 for 48 h and then harvested for analysis. The blot shows restored AMPK phosphorylation in siCKB cells following PF-739 treatment.

(B) Relative mRNA expression of DNL-related genes in human preadipocytes transfected at D-1 with siC or siCKB. At D10 of differentiation, cells were treated with vehicle or PF-739 for 48 h and then harvested for analysis. Data are mean \pm SEM. Statistical significance was assessed by two-way ANOVA with Tukey's multiple-comparison test vs. siC. * p < 0.05, ** p < 0.01, *** p < 0.001, **** p < 0.0001.

(C) Representative immunoblot of cells transfected at D-1 with siC or siCKB, incubated with vehicle or rapamycin for 48 h at D10 of differentiation and harvested afterward for analyses.

(D) Relative mRNA expression of DNL-related gene expression in human preadipocytes transfected at D-1 with siC or siCKB, incubated with vehicle or rapamycin for 48 h at D10 of differentiation and harvested afterward for analyses. Values are mean \pm SEM. p value was calculated using two-way ANOVA and Tukey's multiple-comparison test, comparing all conditions to siC unless indicated otherwise. * p < 0.05, ** p < 0.01, *** p < 0.001, **** p < 0.0001.

(E) On the left, representative immunohistochemical high-throughput quantification of cells transfected at D-1 with siC or siCKB, incubated with vehicle or rapamycin for 48 h at D10 of differentiation, and fixed afterward for analyses. Scale bar represents 20 μ m. On the right, high-throughput quantification of the immunohistochemical BODIPY intensity. Values are relative to Hoechst intensity and represented as mean \pm SEM. p value was calculated using two-way ANOVA and Tukey's multiple-comparison test, comparing all conditions to siC unless indicated otherwise. n > 10 per group, **** p < 0.0001.

(F) Representative immunoblot of immunoprecipitation of endogenous AKT from whole-cell lysates using AKT antibody or IgG control (upper blot), with corresponding input samples shown (lower blot).

(G) Representative immunoblot of human preadipocytes transfected at D-1 with siC or siCKB; incubated at D10 of differentiation with vehicle, MK-2206 (Akt inhibitor), or insulin-starved for 48 h (-INS); and harvested afterward for analyses.

(H) Relative mRNA expression of DNL-related genes in human preadipocytes transfected at D-1 with siC or siCKB, incubated at D10 of differentiation with vehicle or MK-2206 for 48 h, and harvested afterward for analyses. Values are mean \pm SEM. p value was calculated using two-way ANOVA and Tukey's multiple-comparison test, comparing all conditions to siC unless indicated otherwise. * p < 0.05, ** p < 0.01, *** p < 0.001, **** p < 0.0001.

(I) Stimulated DNL assay in cells transfected at D-1 with siC or siCKB, incubated at D10 of differentiation with vehicle or MK-2206 for 48 h, and harvested afterward for analyses. Values are mean \pm SEM. p value was calculated using two-way ANOVA and Tukey's multiple-comparison test, comparing all conditions to siC unless indicated otherwise. ** p < 0.01, *** p < 0.001.

(J) On the left, representative immunohistochemical staining for Hoechst (nuclei) and BODIPY (lipid droplets) in cells transfected at D-1 with siC or siCKB, incubated at D10 of differentiation with vehicle or MK-2206 for 48 h, and fixed afterward for analyses. Scale bar represents 50 μ m. On the right, high-throughput quantification of the immunohistochemical BODIPY intensity. Values are relative to Hoechst intensity and represented as mean \pm SEM. p value was calculated using two-way ANOVA and Tukey's multiple-comparison test, comparing all conditions to siC unless indicated otherwise. n > 10, **** p < 0.0001.

(K) Representative immunoblot in early siC- and siCKB-transfected cells (transfection at D-1) re-transfected at D8 with either mRNA encoding CKB or a non-coding vehicle.

(legend continued on next page)

progressively during adipocyte differentiation and acts independently of the Cr-PCr energy shuttle to constrain insulin-AKT-mTORC1 signaling. Mechanistically, CKB fine-tunes AKT activity by limiting its phosphorylation, thereby attenuating downstream activation of mTORC1, glycolysis, and ChREBP-driven lipogenesis. Loss of CKB enhances AKT phosphorylation only in the presence of insulin, suggesting that CKB specifically modulates growth factor-driven AKT activation. Whether CKB's enzymatic activity, dictated by its structural conformation, affects AKT binding remains unresolved, as the absence of a selective CKB inhibitor currently limits direct testing of this hypothesis.

Within the broader framework of adipose biology, the AKT-mTORC1 axis functions as a central hub for integrating nutrient and growth factor signals, driving both adipogenesis and systemic lipid storage.⁶⁰ Pharmacological inhibition of mTORC1 with rapamycin has been shown to impair both adipogenesis and lipogenesis,^{61–64} and genetic disruption of its components alters adiposity *in vivo*.^{65,66} A primary upstream activator of mTORC1 is the serine/threonine kinase AKT, which promotes cell growth and survival by phosphorylating multiple downstream substrates. In adipocytes, AKT stimulates mTORC1 through phosphorylation of the inhibitory regulators TSC2 and PRAS40, thereby promoting lipid biosynthesis and storage.⁶⁷ While the activation of AKT via receptor tyrosine kinase-PI3K-mTORC2 pathways is well characterized, the molecular mechanisms that negatively regulate AKT activity are less defined and have been largely attributed to phosphatases such as PTEN and PP2A.^{16,68} Our findings extend emerging evidence from T cell biology implicating CKB and creatine metabolism in growth factor-driven anabolic regulation⁴⁵ revealing that, in adipocytes, CKB acts as a protein-based checkpoint that selectively dampens insulin-driven mTORC1 activation, glycolytic flux, and ChREBP-dependent lipogenesis. Mechanistically, our model aligns with oncogenic studies showing that CKB binding can prevent PIP3-dependent AKT activation,^{51,52} consistent with our observation that CKB's effects depend on insulin-mediated PI3K activation.⁶⁹

In the murine model, adipocyte-specific *Ckb* deletion drives DNL in inguinal WAT while sparing epididymal WAT. We propose that this depot-specific effect reflects differences in inflammatory tone and insulin sensitivity: epididymal WAT is chronically inflamed in obesity, a condition impairing insulin signaling and suppressing DNL,^{70–73} thereby masking the absence of CKB's fine-tuning effect on AKT. In contrast, inguinal WAT retains relative insulin sensitivity and has a lower inflammatory burden, enabling CKB depletion to directly enhance AKT-mTORC1 activity and lipogenesis, creating a permissive environment in which CKB depletion directly drives lipogenesis.^{70–73} This model is consistent with human and rodent data linking reduced CKB expression to visceral depot inflammation²⁶ and with reports

that inflammation selectively attenuates DNL in insulin-resistant adipose tissue.^{17,74} In obesity, CKB downregulation correlates with inflammatory status,²⁶ and ER stress-driven IRE1-XBP1s signaling has been implicated in DNMT3A-mediated methylation and silencing of the *CKB* promoter.⁷⁵ We hypothesize that this downregulation may represent a compensatory attempt to boost AKT signaling in the setting of insulin resistance by relieving CKB's inhibitory effect. While such a mechanism could partially restore anabolic signaling, it may also exacerbate adipose dysfunction by amplifying lipogenesis under metabolically unfavorable conditions.

In summary, we identify CKB as a conditional metabolic regulator that integrates nutrient-sensing and insulin signaling pathways to modulate lipogenesis in a depot-specific manner. By directly binding AKT and attenuating insulin-mTORC1-ChREBP signaling, CKB constrains glycolysis and DNL, shaping lipid storage capacity in adipocytes. We propose that CKB functions not as a determinant of differentiation itself but as a metabolic “priming” factor that enables differentiated adipocytes to mount a lipogenic program. Targeting this pathway could allow selective enhancement of lipid storage in metabolically favorable depots while limiting visceral fat accumulation, potentially offering a strategy for improving metabolic health.

Limitations of the study

A limitation of our study is that the full physiological relevance of CKB in murine adipose biology remains incompletely defined. While our data establish a role for CKB in both human and mouse adipocytes and support its *in vivo* importance, the available mouse model introduces interpretive constraints. Adipocyte-specific *Ckb* deletion predisposes mice to obesity but also impairs glucose homeostasis, a phenotype likely driven by defects in brown adipose tissue thermogenesis and WAT inflammation rather than by isolated changes in lipid metabolism.^{22,26} Dissecting CKB's contribution to early adipocyte lineage commitment vs. its function in mature adipocytes will require inducible, progenitor-targeted approaches (e.g., *Pdgfra*^{CreERT2}), which would clearly separate developmental from maintenance roles. However, *Ckb* deletion late in differentiation still increases lipogenesis in inguinal WAT. Moreover, targeting *Ckb* in preadipocytes isolated from murine WAT confirms these findings. Another limitation concerns the depot specificity of the phenotype. Although metabolic and inflammatory differences between adipose depots are well established, the variation in DNL capacity and its regulation across depots remain unclear. Subcutaneous WAT shows higher DNL capacity, which may provide protection against metabolic disorders.⁷⁶ This difference may partly reflect the relative enrichment of subcutaneous depots with classical adipocytes, which are specialized in lipid metabolism.⁷⁷ Further studies using adipocytes isolated from each depot are needed to

(L) Relative mRNA expression of DNL-related genes in early siC- and siCKB-transfected cells (transfection at D-1) re-transfected at D8 of differentiation with either mRNA encoding *CKB* or a non-coding vehicle. Values are mean \pm SEM. *p* value was calculated using two-way ANOVA and Tukey's multiple-comparison test, comparing all conditions to siC unless indicated otherwise. ****p* < 0.001, *****p* < 0.0001.

(M) Representative immunohistochemical high-throughput quantification of early siC- and siCKB-transfected cells (transfection at D-1) re-transfected at D8 of differentiation with either mRNA encoding *CKB* or a non-coding vehicle. Values are relative to Hoechst intensity and represented as mean \pm SEM. *p* value was calculated using two-way ANOVA and Tukey's multiple-comparison test, comparing all conditions to siC unless indicated otherwise. *n* > 10, ***p* < 0.01.

define the depot-specific roles of creatine metabolism and CKB in adipocyte function.

RESOURCE AVAILABILITY

Lead contact

Requests for further information and resources should be directed to and will be fulfilled by the lead contact Salwan Maqdasy (salwan.maqdasy@ki.se).

Materials availability

This study did not generate new unique reagents.

Data and code availability

- RNA-seq data have been deposited at GEO and are publicly available as of the date of publication (accession GEO: GSE307820).
- This paper does not report original code.
- Additional information is available from the [lead contact](#) upon request.

ACKNOWLEDGMENTS

We would like to thank Prof. Mikael Rydén and Dr. Niklas Mejhert for their scientific inputs, supervision, and guidance of this work. Prof. Mikael Rydén designed and supervised the clinical studies where data have been used in this manuscript. We would also like to thank Prof. Karine Clément for her scientific inputs. Additionally, we would like to thank Prof. Martin O. Bergö for allowing us to use the high-resolution respirometry equipment employed in the study. We would like to thank Dr. Lawrence Kazak and Dr. Bozena Samborska who generously provided samples from mice generated at their lab (McGill, Montreal, Canada). We would like to thank Prof. Ez-Zoubir Amri who generously provided hMADS.

Funding sources: S.M. is supported by CIMED, European Foundation for the Study of Diabetes Rising Star award, and Swedish Research Council. S.L. is supported by the French National Agency for Research, ANR-AGAAT, and Association Française d'Étude et de Recherche sur l'obésité (AFERO). B.A. and A.A.B. are supported by the European Research Council (ERC Synergy grant SPHERES # 856404).

AUTHOR CONTRIBUTIONS

Conceptualization, G.R., S.L., and S.M.; methodology, G.R., J.F.R., G.M., B.A., S.L., and S.M.; investigation, G.R., R.H., A.A.B., M.O.-H., I.V., M.H., L.M., F.M., C.R., O.H., J.F.R., S.L., and S.M.; writing – original draft, G.R., S.L., and S.M.; writing – review & editing, G.R., S.L., and S.M.; funding acquisition, S.L. and S.M.; and supervision, S.L. and S.M. All the coauthors read and approved the article.

DECLARATION OF INTERESTS

The authors declare no competing interests.

STAR★METHODS

Detailed methods are provided in the online version of this paper and include the following:

- **KEY RESOURCES TABLE**
- **EXPERIMENTAL MODEL AND SUBJECT DETAILS**
 - Subjects
 - Cell cultures
 - Animals
- **METHOD DETAILS**
 - RNA isolation, cDNA synthesis and real-time qPCR
 - *In vitro* transcription and mRNA-based re-expression
 - CRISPRa for endogenous CKB overexpression
 - RNAi and re-expression experiments at D3 and D8
 - Early transfection of pre-adipocytes (D-1) and incubations with chemicals

- Library preparation and RNA sequencing
- Western Blot analysis
- Immunoprecipitation from whole lysate
- ATP measurement
- Metabolomic samples preparation and targeted metabolomic measurements
- Creatine kinase activity
- ELISA assays
- Triglyceride extraction and measurement
- Immunofluorescence (IF)
- Confocal microscopy
- Quantification of lipid accumulation (by Bodipy staining)
- Seahorse assays
- Radioactive *de novo* lipogenesis measurement
- Radioactive glucose uptake measurement
- **QUANTIFICATION AND STATISTICAL ANALYSIS**

SUPPLEMENTAL INFORMATION

Supplemental information can be found online at <https://doi.org/10.1016/j.celrep.2025.116489>.

Received: November 8, 2024

Revised: August 21, 2025

Accepted: October 6, 2025

REFERENCES

1. Olzmann, J.A., and Carvalho, P. (2019). Dynamics and functions of lipid droplets. *Nat. Rev. Mol. Cell Biol.* 20, 137–155. <https://doi.org/10.1038/s41580-018-0085-z>.
2. Pellegrinelli, V., Carobbio, S., and Vidal-Puig, A. (2016). Adipose tissue plasticity: how fat depots respond differently to pathophysiological cues. *Diabetologia* 59, 1075–1088. <https://doi.org/10.1007/s00125-016-3933-4>.
3. Petersen, M.C., and Shulman, G.I. (2018). Mechanisms of Insulin Action and Insulin Resistance. *Physiol. Rev.* 98, 2133–2223. <https://doi.org/10.1152/physrev.00063.2017>.
4. Kawahito, S., Kitahata, H., and Oshita, S. (2009). Problems associated with glucose toxicity: role of hyperglycemia-induced oxidative stress. *World J. Gastroenterol.* 15, 4137–4142. <https://doi.org/10.3748/wjg.15.4137>.
5. Blüher, M. (2020). Metabolically Healthy Obesity. *Endocr. Rev.* 41, bnaa004. <https://doi.org/10.1210/edrv/bnaa004>.
6. Ghaben, A.L., and Scherer, P.E. (2019). Adipogenesis and metabolic health. *Nat. Rev. Mol. Cell Biol.* 20, 242–258. <https://doi.org/10.1038/s41580-018-0093-z>.
7. Lecoutre, S., Rebière, C., Maqdasy, S., Lambert, M., Dussaud, S., Abatan, J.B., Dugail, I., Gautier, E.L., Clément, K., and Marcelin, G. (2025). Enhancing adipose tissue plasticity: progenitor cell roles in metabolic health. *Nat. Rev. Endocrinol.* 21, 272–288. <https://doi.org/10.1038/s41574-024-01071-y>.
8. Cotillard, A., Poitou, C., Torcivia, A., Bouillot, J.-L., Dietrich, A., Klötting, N., Grégoire, C., Lolmede, K., Blüher, M., and Clément, K. (2014). Adipocyte size threshold matters: link with risk of type 2 diabetes and improved insulin resistance after gastric bypass. *J. Clin. Endocrinol. Metab.* 99, E1466–E1470. <https://doi.org/10.1210/jc.2014-1074>.
9. Mikkelsen, T.S., Xu, Z., Zhang, X., Wang, L., Gimble, J.M., Lander, E.S., and Rosen, E.D. (2010). Comparative epigenomic analysis of murine and human adipogenesis. *Cell* 143, 156–169. <https://doi.org/10.1016/j.cell.2010.09.006>.
10. Lefterova, M.I., Haakonsson, A.K., Lazar, M.a., and Mandrup, S. (2014). PPAR gamma and the global map of adipogenesis and beyond. *Trends Endocrinol. Metab.* 25, 293–302. <https://doi.org/10.1016/j.tem.2014.04.001>.

11. Smith, U., and Kahn, B.B. (2016). Adipose tissue regulates insulin sensitivity: role of adipogenesis, de novo lipogenesis and novel lipids. *J. Intern. Med.* 280, 465–475. <https://doi.org/10.1111/joim.12540>.
12. Collins, J.M., Neville, M.J., Pinnick, K.E., Hodson, L., Ruyter, B., van Dijk, T.H., Reijngoud, D.-J., Fielding, M.D., and Frayn, K.N. (2011). De novo lipogenesis in the differentiating human adipocyte can provide all fatty acids necessary for maturation. *J. Lipid Res.* 52, 1683–1692. <https://doi.org/10.1194/jlr.M012195>.
13. Dunlop, M., and Court, J.M. (1978). Lipogenesis in developing human adipose tissue. *Early Hum. Dev.* 2, 123–130. [https://doi.org/10.1016/0378-3782\(78\)90004-x](https://doi.org/10.1016/0378-3782(78)90004-x).
14. Couchet, M., Gao, H., Klingelhuber, F., Jalkanen, J., De Castro Barbosa, T., Omar-Hmeadi, M., Massier, L., Krahmer, N., Mejhert, N., and Rydén, M. (2025). Adipogenic characterization of immortalized CD55+ progenitor cells from human white adipose tissue. *Adipocyte* 14, 2283213. <https://doi.org/10.1080/21623945.2023.2283213>.
15. Donnelly, K.L., Smith, C.I., Schwarzenberg, S.J., Jessurun, J., Boldt, M.D., and Parks, E.J. (2005). Sources of fatty acids stored in liver and secreted via lipoproteins in patients with nonalcoholic fatty liver disease. *J. Clin. Invest.* 115, 1343–1351. <https://doi.org/10.1172/JCI23621>.
16. Tang, Y., Wallace, M., Sanchez-Gurmaches, J., Hsiao, W.-Y., Li, H., Lee, P.L., Vernia, S., Metallo, C.M., and Guertin, D.A. (2016). Adipose tissue mTORC2 regulates ChREBP-driven de novo lipogenesis and hepatic glucose metabolism. *Nat. Commun.* 7, 11365. <https://doi.org/10.1038/ncomms11365>.
17. Hsiao, W.-Y., and Guertin, D.A. (2019). De Novo Lipogenesis as a Source of Second Messengers in Adipocytes. *Curr. Diab. Rep.* 19, 138. <https://doi.org/10.1007/s11892-019-1264-9>.
18. Green, C.R., Wallace, M., Divakaruni, A.S., Phillips, S.A., Murphy, A.N., Ciaraldi, T.P., and Metallo, C.M. (2016). Branched-chain amino acid catabolism fuels adipocyte differentiation and lipogenesis. *Nat. Chem. Biol.* 12, 15–21. <https://doi.org/10.1038/nchembio.1961>.
19. Zaganjor, E., Yoon, H., Spinelli, J.B., Nunn, E.R., Laurent, G., Keskinidis, P., Sivaloganathan, S., Joshi, S., Notarangelo, G., Mulei, S., et al. (2021). SIRT4 is an early regulator of branched-chain amino acid catabolism that promotes adipogenesis. *Cell Rep.* 36, 109345. <https://doi.org/10.1016/j.celrep.2021.109345>.
20. Green, C.R., Alaeddine, L.M., Wessendorf-Rodriguez, K.A., Turner, R., Elmastas, M., Hover, J.D., Murphy, A.N., Ryden, M., Mejhert, N., Metallo, C.M., and Wallace, M. (2024). Impaired branched-chain amino acid (BCAA) catabolism during adipocyte differentiation decreases glycolytic flux. *J. Biol. Chem.* 300, 108004. <https://doi.org/10.1016/j.jbc.2024.108004>.
21. Kazak, L., and Cohen, P. (2020). Creatine metabolism: energy homeostasis, immunity and cancer biology. *Nat. Rev. Endocrinol.* 16, 421–436. <https://doi.org/10.1038/s41574-020-0365-5>.
22. Rahbani, J.F., Roesler, A., Hussain, M.F., Samborska, B., Dykstra, C.B., Tsai, L., Jedrychowski, M.P., Vergnes, L., Reue, K., Spiegelman, B.M., and Kazak, L. (2021). Creatine kinase B controls futile creatine cycling in thermogenic fat. *Nature* 590, 480–485. <https://doi.org/10.1038/s41586-021-03221-y>.
23. Rahbani, J.F., Bunk, J., Lagarde, D., Samborska, B., Roesler, A., Xiao, H., Shaw, A., Kaiser, Z., Braun, J.L., Geromella, M.S., et al. (2024). Parallel control of cold-triggered adipocyte thermogenesis by UCP1 and CKB. *Cell Metab.* 36, 526–540.e7. <https://doi.org/10.1016/j.cmet.2024.01.001>.
24. Bunk, J., Ersin, M., Hussain, M.F., Samborska, B., Guerra-Martinez, M., Soni, D., and Kazak, L. (2025). Creatine kinase B mediates UCP1-independent beige fat thermogenesis via the futile creatine cycle in mice. *Mol. Metab.* 98, 102193. <https://doi.org/10.1016/j.molmet.2025.102193>.
25. Kazak, L., Chouchani, E.T., Jedrychowski, M.P., Erickson, B.K., Shinoda, K., Cohen, P., Vetrivelan, R., Lu, G.Z., Laznik-Bogoslavski, D., Hasenfuss, S.C., et al. (2015). A creatine-driven substrate cycle enhances energy expenditure and thermogenesis in beige fat. *Cell* 163, 643–655. <https://doi.org/10.1016/j.cell.2015.09.035>.
26. Maqdasy, S., Lecoutre, S., Renzi, G., Frendo-Cumbo, S., Rizo-Roca, D., Moritz, T., Juvany, M., Hodek, O., Gao, H., Couchet, M., et al. (2022). Impaired phosphocreatine metabolism in white adipocytes promotes inflammation. *Nat. Metab.* 4, 190–202. <https://doi.org/10.1038/s42255-022-00525-9>.
27. Arner, E., Daub, C.O., Vitting-Seerup, K., Andersson, R., Lilje, B., Drablos, F., Lennartsson, A., Rönnerblad, M., Hrydzusko, O., Vitezić, M., et al. (2015). Transcribed enhancers lead waves of coordinated transcription in transitioning mammalian cells. *Science* 347, 1010–1014. <https://doi.org/10.1126/science.1259418>.
28. Petrus, P., Lecoutre, S., Dollet, L., Wiel, C., Sulen, A., Gao, H., Tavira, B., Laurencikienė, J., Rooyackers, O., Checa, A., et al. (2020). Glutamine Links Obesity to Inflammation in Human White Adipose Tissue. *Cell Metab.* 31, 375–390.e11. <https://doi.org/10.1016/j.cmet.2019.11.019>.
29. Pan, X., Ye, L., Guo, X., Wang, W., Zhang, Z., Wang, Q., Huang, J., Xu, J., Cai, Y., Shou, X., et al. (2023). Glutamine Production by Glut Promotes Thermogenic Adipocyte Differentiation Through Prdm9-Mediated H3K4me3 and Transcriptional Reprogramming. *Diabetes* 72, 1574–1596. <https://doi.org/10.2337/db23-0162>.
30. Lecoutre, S., Maqdasy, S., Rizo-Roca, D., Renzi, G., Vlassakev, I., Alaeddine, L.M., Higos, R., Jalkanen, J., Zhong, J., Zareifi, D.S., et al. (2024). Reduced adipocyte glutaminase activity promotes energy expenditure and metabolic health. *Nat. Metab.* 6, 1329–1346. <https://doi.org/10.1038/s42255-024-01083-y>.
31. Klingelhuber, F., Frendo-Cumbo, S., Omar-Hmeadi, M., Massier, L., Kakimoto, P., Taylor, A.J., Couchet, M., Ribicic, S., Wabitsch, M., Messias, A.C., et al. (2024). A spatiotemporal proteomic map of human adipogenesis. *Nat. Metab.* 6, 861–879. <https://doi.org/10.1038/s42255-024-01025-8>.
32. Zhong, J., Zareifi, D., Weinbrenner, S., Hansen, M., Klingelhuber, F., Nono Nankam, P.A., Frendo-Cumbo, S., Bhalla, N., Cordeddu, L., de Castro Barbosa, T., et al. (2025). adiposetissue.org: A knowledge portal integrating clinical and experimental data from human adipose tissue. *Cell Metab.* 37, 566–569. <https://doi.org/10.1016/j.cmet.2025.01.012>.
33. Bäckdahl, J., Franzén, L., Massier, L., Li, Q., Jalkanen, J., Gao, H., Andersson, A., Bhalla, N., Thorell, A., Rydén, M., et al. (2021). Spatial mapping reveals human adipocyte subpopulations with distinct sensitivities to insulin. *Cell Metab.* 33, 1869–1882.e6. <https://doi.org/10.1016/j.cmet.2021.07.018>.
34. Seppet, E.K., and Saks, V.A. (1994). Thyroid hormones and the creatine kinase system in cardiac cells. *Mol. Cell. Biochem.* 133–134, 299–309. <https://doi.org/10.1007/BF01267962>.
35. Arner, E., Mejhert, N., Kulyté, A., Balwier, P.J., Pachkov, M., Cormont, M., Lorente-Cebrián, S., Ehrlund, A., Laurencikienė, J., Hedén, P., et al. (2012). Adipose tissue microRNAs as regulators of CCL2 production in human obesity. *Diabetes* 61, 1986–1993. <https://doi.org/10.2337/db11-1508>.
36. Rodriguez, A.-M., Elabd, C., Amri, E.-Z., Ailhaud, G., and Dani, C. (2005). The human adipose tissue is a source of multipotent stem cells. *Biochimie* 87, 125–128. <https://doi.org/10.1016/j.biochi.2004.11.007>.
37. Yore, M.M., Syed, I., Moraes-Vieira, P.M., Zhang, T., Herman, M.A., Homan, E.A., Patel, R.T., Lee, J., Chen, S., Peroni, O.D., et al. (2014). Discovery of a class of endogenous mammalian lipids with anti-diabetic and anti-inflammatory effects. *Cell* 159, 318–332. <https://doi.org/10.1016/j.cell.2014.09.035>.
38. Uyeda, K., and Repa, J.J. (2006). Carbohydrate response element binding protein, ChREBP, a transcription factor coupling hepatic glucose utilization and lipid synthesis. *Cell Metab.* 4, 107–110. <https://doi.org/10.1016/j.cmet.2006.06.008>.
39. Herman, M.A., Peroni, O.D., Villoria, J., Schön, M.R., Abumrad, N.A., Blüher, M., Klein, S., and Kahn, B.B. (2012). A novel ChREBP isoform in adipose tissue regulates systemic glucose metabolism. *Nature* 484, 333–338. <https://doi.org/10.1038/nature10986>.

40. Dentin, R., Langin, D., and Postic, C. (2012). Hidden variant of ChREBP in fat links lipogenesis to insulin sensitivity. *Cell Metab.* 15, 795–797. <https://doi.org/10.1016/j.cmet.2012.05.007>.
41. Li, M.V., Chang, B., Imamura, M., Pongvarin, N., and Chan, L. (2006). Glucose-dependent transcriptional regulation by an evolutionarily conserved glucose-sensing module. *Diabetes* 55, 1179–1189. <https://doi.org/10.2337/db05-0822>.
42. Zhang, D., Li, J., Wang, F., Hu, J., Wang, S., and Sun, Y. (2014). 2-Deoxy-D-glucose targeting of glucose metabolism in cancer cells as a potential therapy. *Cancer Lett.* 355, 176–183. <https://doi.org/10.1016/j.canlet.2014.09.003>.
43. Ponticos, M., Lu, Q.L., Morgan, J.E., Hardie, D.G., Partridge, T.A., and Carling, D. (1998). Dual regulation of the AMP-activated protein kinase provides a novel mechanism for the control of creatine kinase in skeletal muscle. *EMBO J.* 17, 1688–1699. <https://doi.org/10.1093/emboj/17.6.1688>.
44. Steinberg, G.R., and Hardie, D.G. (2023). New insights into activation and function of the AMPK. *Nat. Rev. Mol. Cell Biol.* 24, 255–272. <https://doi.org/10.1038/s41580-022-00547-x>.
45. Samborska, B., Roy, D.G., Rahbani, J.F., Hussain, M.F., Ma, E.H., Jones, R.G., and Kazak, L. (2022). Creatine transport and creatine kinase activity is required for CD8+ T cell immunity. *Cell Rep.* 38, 110446. <https://doi.org/10.1016/j.celrep.2022.110446>.
46. Sengupta, S., Peterson, T.R., and Sabatini, D.M. (2010). Regulation of the mTOR complex 1 pathway by nutrients, growth factors, and stress. *Mol. Cell* 40, 310–322. <https://doi.org/10.1016/j.molcel.2010.09.026>.
47. Sabatini, D.M., Erdjument-Bromage, H., Lui, M., Tempst, P., and Snyder, S.H. (1994). RAFT1: a mammalian protein that binds to FKBP12 in a rapamycin-dependent fashion and is homologous to yeast TORs. *Cell* 78, 35–43. [https://doi.org/10.1016/0092-8674\(94\)90570-3](https://doi.org/10.1016/0092-8674(94)90570-3).
48. Brown, E.J., Albers, M.W., Shin, T.B., Ichikawa, K., Keith, C.T., Lane, W.S., and Schreiber, S.L. (1994). A mammalian protein targeted by G1-arresting rapamycin-receptor complex. *Nature* 369, 756–758. <https://doi.org/10.1038/369756a0>.
49. Kimball, S.R., and Jefferson, L.S. (2006). Signaling pathways and molecular mechanisms through which branched-chain amino acids mediate translational control of protein synthesis. *J. Nutr.* 136, 227S–231S. <https://doi.org/10.1093/jn/136.1.227S>.
50. Laplante, M., and Sabatini, D.M. (2012). mTOR signaling in growth control and disease. *Cell* 149, 274–293. <https://doi.org/10.1016/j.cell.2012.03.017>.
51. He, L., Lin, J., Lu, S., Li, H., Chen, J., Wu, X., Yan, Q., Liu, H., Li, H., and Shi, Y. (2024). CKB Promotes Mitochondrial ATP Production by Suppressing Permeability Transition Pore. *Adv. Sci.* 11, e2403093. <https://doi.org/10.1002/adv.202403093>.
52. Wang, Z., Hulsurkar, M., Zhuo, L., Xu, J., Yang, H., Naderinezhad, S., Wang, L., Zhang, G., Ai, N., Li, L., et al. (2021). CKB inhibits epithelial-mesenchymal transition and prostate cancer progression by sequestering and inhibiting AKT activation. *Neoplasia* 23, 1147–1165. <https://doi.org/10.1016/j.neo.2021.09.005>.
53. Hirai, H., Sootome, H., Nakatsuru, Y., Miyama, K., Taguchi, S., Tsujioka, K., Ueno, Y., Hatch, H., Majumder, P.K., Pan, B.-S., and Kotani, H. (2010). MK-2206, an allosteric Akt inhibitor, enhances antitumor efficacy by standard chemotherapeutic agents or molecular targeted drugs in vitro and in vivo. *Mol. Cancer Ther.* 9, 1956–1967. <https://doi.org/10.1158/1535-7163.MCT-09-1012>.
54. Whiteman, E.L., Cho, H., and Birnbaum, M.J. (2002). Role of Akt/protein kinase B in metabolism. *Trends Endocrinol. Metab.* 13, 444–451. [https://doi.org/10.1016/s1043-2760\(02\)00662-8](https://doi.org/10.1016/s1043-2760(02)00662-8).
55. Vishvanath, L., and Gupta, R.K. (2019). Contribution of adipogenesis to healthy adipose tissue expansion in obesity. *J. Clin. Investig.* 129, 4022–4031. <https://doi.org/10.1172/JCI129191>.
56. Kim, J.B., and Spiegelman, B.M. (1996). ADD1/SREBP1 promotes adipocyte differentiation and gene expression linked to fatty acid metabolism. *Genes Dev.* 10, 1096–1107. <https://doi.org/10.1101/gad.10.9.1096>.
57. Ameer, F., Scanduzzi, L., Hasnain, S., Kalbacher, H., and Zaidi, N. (2014). De novo lipogenesis in health and disease. *Metabolism* 63, 895–902. <https://doi.org/10.1016/j.metabol.2014.04.003>.
58. Deminice, R., da Silva, R.P., Lamarre, S.G., Brown, C., Furey, G.N., McCarter, S.A., Jordao, A.A., Kelly, K.B., King-Jones, K., Jacobs, R.L., et al. (2011). Creatine supplementation prevents the accumulation of fat in the livers of rats fed a high-fat diet. *J. Nutr.* 141, 1799–1804. <https://doi.org/10.3945/jn.111.144857>.
59. Deminice, R., de Castro, G.S.F., Francisco, L.V., da Silva, L.E.C.M., Cardoso, J.F.R., Frajacom, F.T.T., Teodoro, B.G., Dos Reis Silveira, L., and Jordao, A.A. (2015). Creatine supplementation prevents fatty liver in rats fed choline-deficient diet: a burden of one-carbon and fatty acid metabolism. *J. Nutr. Biochem.* 26, 391–397. <https://doi.org/10.1016/j.jnutbio.2014.11.014>.
60. He, L., Cho, S., and Blenis, J. (2025). mTORC1, the maestro of cell metabolism and growth. *Genes Dev.* 39, 109–131. <https://doi.org/10.1101/gad.352084.124>.
61. Yeh, W.C., Bierer, B.E., and McKnight, S.L. (1995). Rapamycin inhibits clonal expansion and adipogenic differentiation of 3T3-L1 cells. *Proc. Natl. Acad. Sci. USA* 92, 11086–11090. <https://doi.org/10.1073/pnas.92.24.11086>.
62. Bell, A., Grunder, L., and Sorisky, A. (2000). Rapamycin inhibits human adipocyte differentiation in primary culture. *Obes. Res.* 8, 249–254. <https://doi.org/10.1038/oby.2000.29>.
63. Gagnon, A., Lau, S., and Sorisky, A. (2001). Rapamycin-sensitive phase of 3T3-L1 preadipocyte differentiation after clonal expansion. *J. Cell. Physiol.* 189, 14–22. <https://doi.org/10.1002/jcp.1132>.
64. Kim, J.E., and Chen, J. (2004). regulation of peroxisome proliferator-activated receptor-gamma activity by mammalian target of rapamycin and amino acids in adipogenesis. *Diabetes* 53, 2748–2756. <https://doi.org/10.2337/diabetes.53.11.2748>.
65. Um, S.H., Frigerio, F., Watanabe, M., Picard, F., Joaquin, M., Sticker, M., Fumagalli, S., Allegrini, P.R., Kozma, S.C., Auwerx, J., and Thomas, G. (2004). Absence of S6K1 protects against age- and diet-induced obesity while enhancing insulin sensitivity. *Nature* 431, 200–205. <https://doi.org/10.1038/nature02866>.
66. Le Bacquer, O., Petroulakis, E., Pagliarunga, S., Poulin, F., Richard, D., Cianflone, K., and Sonenberg, N. (2007). Elevated sensitivity to diet-induced obesity and insulin resistance in mice lacking 4E-BP1 and 4E-BP2. *J. Clin. Investig.* 117, 387–396. <https://doi.org/10.1172/JCI29528>.
67. Manning, B.D., and Cantley, L.C. (2007). AKT/PKB signaling: navigating downstream. *Cell* 129, 1261–1274. <https://doi.org/10.1016/j.cell.2007.06.009>.
68. Manning, B.D., and Toker, A. (2017). AKT/PKB Signaling: Navigating the Network. *Cell* 169, 381–405. <https://doi.org/10.1016/j.cell.2017.04.001>.
69. Harrington, L.S., Findlay, G.M., and Lamb, R.F. (2005). Restraining PI3K: mTOR signalling goes back to the membrane. *Trends Biochem. Sci.* 30, 35–42. <https://doi.org/10.1016/j.tibs.2004.11.003>.
70. Wueest, S., Schoenle, E.J., and Konrad, D. (2012). Depot-specific differences in adipocyte insulin sensitivity in mice are diet- and function-dependent. *Adipocyte* 1, 153–156. <https://doi.org/10.4161/adip.19910>.
71. Mileti, E., Kwok, K.H.M., Andersson, D.P., Mathelier, A., Raman, A., Bäckdahl, J., Jalkanen, J., Massier, L., Thorell, A., Gao, H., et al. (2021). Human White Adipose Tissue Displays Selective Insulin Resistance in the Obese State. *Diabetes* 70, 1486–1497. <https://doi.org/10.2337/db21-0001>.
72. Samaras, K., Botelho, N.K., Chisholm, D.J., and Lord, R.V. (2010). Subcutaneous and visceral adipose tissue gene expression of serum adipokines that predict type 2 diabetes. *Obes. Silver Spring Md* 18, 884–889. <https://doi.org/10.1038/oby.2009.443>.

73. Song, M.-G., Lee, H.-J., Jin, B.-Y., Gutierrez-Aguilar, R., Shin, K.-H., Choi, S.-H., Um, S.H., and Kim, D.-H. (2016). Depot-specific differences in angiogenic capacity of adipose tissue in differential susceptibility to diet-induced obesity. *Mol. Metab.* 5, 1113–1120. <https://doi.org/10.1016/j.molmet.2016.09.001>.
74. Cawthorn, W.P., and Sethi, J.K. (2008). TNF-alpha and adipocyte biology. *FEBS Lett.* 582, 117–131. <https://doi.org/10.1016/j.febslet.2007.11.051>.
75. Renzi, G., Vlassakev, I., Hansen, M., Higos, R., Lecoutre, S., Elmastas, M., Hodek, O., Moritz, T., Alaeddine, L.M., Frendo-Cumbo, S., et al. (2025). Epigenetic suppression of creatine kinase B in adipocytes links endoplasmic reticulum stress to obesity-associated inflammation. *Mol. Metab.* 92, 102082. <https://doi.org/10.1016/j.molmet.2024.102082>.
76. Dobre, M.-Z., Virgolici, B., and Timnea, O. (2025). Key Roles of Brown, Subcutaneous, and Visceral Adipose Tissues in Obesity and Insulin Resistance. *Curr. Issues Mol. Biol.* 47, 343. <https://doi.org/10.3390/cimb47050343>.
77. Lazarescu, O., Ziv-Agam, M., Haim, Y., Hekselman, I., Jubran, J., Shneyour, A., Muallem, H., Zemer, A., Rosengarten-Levin, M., Kitsberg, D., et al. (2025). Human subcutaneous and visceral adipocyte atlases uncover classical and nonclassical adipocytes and depot-specific patterns. *Nat. Genet.* 57, 413–426. <https://doi.org/10.1038/s41588-024-02048-3>.
78. Schauer, N., Steinhauser, D., Strelkov, S., Schomburg, D., Allison, G., Moritz, T., Lundgren, K., Roessner-Tunali, U., Forbes, M.G., Willmitzer, L., et al. (2005). GC-MS libraries for the rapid identification of metabolites in complex biological samples. *FEBS Lett.* 579, 1332–1337. <https://doi.org/10.1016/j.febslet.2005.01.029>.
79. Hofwimmer, K., de Paula Souza, J., Subramanian, N., Vujčić, M., Rachid, L., Méreau, H., Zhao, C., Dror, E., Barreby, E., Björkström, N.K., et al. (2024). IL-1 β promotes adipogenesis by directly targeting adipocyte precursors. *Nat. Commun.* 15, 7957. <https://doi.org/10.1038/s41467-024-51938-x>.

STAR★METHODS

KEY RESOURCES TABLE

| REAGENT or RESOURCE | SOURCE | IDENTIFIER |
|--|---------------------------|----------------------------------|
| Antibodies | | |
| Rabbit IgG-HRP | Sigma-Aldrich | Cat#A9169; RRID: AB_258434 |
| Mouse IgG-HRP | Sigma-Aldrich | Cat#5278; RRID: AB_258232 |
| CKB (for western blot) | Proteintech | Cat#15137-1-AP; RRID:AB_2080878 |
| CKB (for immunofluorescence) | Abcam | Cat#AB151579 |
| CKMT2 | Abcam | Cat#AB55963; RRID:AB_2081191 |
| B-Actin | Sigma-Aldrich | Cat#A5441; RRID:AB_476744 |
| P-ACC | Cell Signaling Technology | Cat#3661; RRID:AB_330337 |
| FASN | Cell Signaling Technology | Cat#3180; RRID:AB_2100796 |
| Vinculin | Santa Cruz Antibodies | Cat# sc-73614; RRID: AB_1131294 |
| P-P70S6K | Cell Signaling Technology | Cat#9205; RRID:AB_330944 |
| P70S6K | Cell Signaling Technology | Cat#2708; RRID:AB_390722 |
| P-AKT 308 | Cell Signaling Technology | Cat#9275; RRID:AB_329828 |
| P-AKT 473 | Cell Signaling Technology | Cat#4060; RRID:AB_2315049 |
| AKT | Cell Signaling Technology | Cat#9272; RRID:AB_329827 |
| P-AMPK | Cell Signaling Technology | Cat#2535; RRID:AB_331250 |
| ChREBP | Novus Biological | Cat#NB400-135; RRID: AB_10002435 |
| Tubulin | Cell Signaling Technology | Cat#2125; RRID:AB_2619646 |
| Calnexin | Cell Signaling Technology | Cat#2679; RRID:AB_2228381 |
| PPARG | Cell Signaling Technology | Cat#2435; RRID:AB_2166051 |
| CEBPA | Cell Signaling Technology | Cat#8178; RRID:AB_11178517 |
| FABP4 | Atlas Antibodies | Cat#HPA002188; RRID: AB_1078822 |
| ADIPOQ | Thermo Fisher Scientific | Cat#MA1-054; RRID: AB_557516 |
| PLIN1 | Cell Signaling Technology | Cat#9349; RRID:AB_10829911 |
| HSL | Cell Signaling Technology | Cat#4107; RRID:AB_2296900 |
| AMPK | Cell Signaling Technology | Cat#2532; RRID:AB_330331 |
| SREBP1 (for immunofluorescence) | Santa Cruz Antibodies | Cat#sc-365513; RRID: AB_10843812 |
| Donkey anti-Mouse IgG (H + L) Highly Cross-Absorbed Secondary Antibody Alexa Fluor 647 | Thermo Fisher Scientific | Cat#A31571; RRID:AB_162542 |
| Goat anti-Rabbit IgG (H + L) Highly Cross-Absorbed Secondary Antibody Alexa Fluor 488 | Thermo Fisher Scientific | Cat#A11008; RRID:AB_143165 |
| Gene silencers | | |
| ON-TARGETplus Non-targeting Pool | Dharmacon | Cat#D-001810-01-20 |
| ON-TARGETplus siRNA CKB - Human | Dharmacon | Cat#L-006706-00-0005 |
| ON-TARGETplus siRNA CKMT2 - Human | Dharmacon | Cat#L-006709-00-0005 |
| ON-TARGETplus siRNA MLXIPL - Human | Dharmacon | Cat#L-009253-00-0005 |
| ON-TARGETplus siRNA Ckb - Mouse | Dharmacon | Cat#L-062038-00-0005 |
| Critical Commercial Assays | | |
| iScript cDNA Synthesis kit | Bio-Rad | Cat#170-8891 |
| Pierce BCA Protein Assay kit | Thermo Fisher Scientific | Cat#23227 |
| HiScribe T7 ARCA mRNA kit (with tailing) | New England Biolabs (NEB) | Cat#E2060S |
| Seahorse XF Mito Stress Test | Agilent | Cat#103015-100 |
| Seahorse XF Glycolysis Stress Test | Agilent | Cat#103020-100 |
| Human Total Adiponectin/Acrp30 Quantikine ELISA | R&D systems | Cat#DRP300 |
| Lactate-Glo™ Assay | Promega | Cat#J5021 |

(Continued on next page)

Continued

| REAGENT or RESOURCE | SOURCE | IDENTIFIER |
|---|---------------------------|-------------------|
| Triglyceride quantification assay-Colorimetric/fluorometric kit | Sigma-Aldrich | Cat#MAK266-1KT |
| ATP Determination Kit | Thermo Fisher Scientific | Cat#A22066 |
| Pierce E-Zinc Reversible Stain kit | Thermo Fisher Scientific | Cat#24582 |
| HiScribe T7 ARCA mRNA kit (with tailing) | New England Biolabs (NEB) | Cat#E2060S |
| NucleoSpin RNA, Mini kit for RNA purification | Macherey-Nagel | Cat#32-740955.250 |
| Invitrogen Neon Transfection System 100 μ L | ThermoFisher | Cat#10114334 |
| Dneasy Blood & Tissue Kit | Qiagen | Cat#69504 |
| NucleoSpin Gel and PCR Clean-up | Macherey-Nagel | Cat#740609.250 |
| Chemicals, Peptides, and Recombinant Proteins | | |
| DharmaFECT 3 Transfection Reagent | Horizon Discovery | Cat#T-2003-03 |
| DMEM 1.0g/L Glucose w/o L-Gln | Lonza | Cat#12-707F |
| SYBR-green Master Mix | Bio-Rad | Cat#1708884 |
| Amersham ECL Prime Western Blotting Detection Reagent | GE Healthcare | Cat#RPN2232 |
| Blotto Immunoanalytical Grade (Non-Fat Dry Milk) | BioNordika | Cat#B501-0500 |
| DTT | Sigma-Aldrich | Cat#10197777001 |
| 2-Mercaptoethanol | Sigma-Aldrich | Cat#M3148-100ML |
| RIPA buffer | Thermo Fisher Scientific | Cat#89901 |
| FGF2 human | Sigma-Aldrich | Cat#F0291 |
| Insulin (liquid, ready to use, 10mg/ml, 5mL) | Sigma-Aldrich | Cat#I9278 |
| T3 | Sigma-Aldrich | Cat#T6397 |
| Transferrin | Sigma-Aldrich | Cat#T8158 |
| IBMX (3-Isobutyl-1-methylxanthin) | Sigma-Aldrich | Cat#I5879 |
| Rosiglitazone (100 mg) | Cayman Chemicals | Cat#71740 |
| Dexamethasone | Sigma-Aldrich | Cat#D1756 |
| 0.5% Trypsin/EDTA (10x) | Invitrogen (GIBCO) | Cat#15400-054 |
| Penicilline G 10000U/ml/Streptomycine 10000 μ g/ml | Invitrogen (GIBCO) | Cat#15140-122 |
| HEPES 1M | Invitrogen (GIBCO) | Cat#15630-056 |
| Ham's F-12 Nutrient Mix | Invitrogen (GIBCO) | Cat#21765-037 |
| DMEM, low glucose, pyruvate (+glutamine) | Invitrogen (GIBCO) | Cat#31885-023 |
| 4x Laemmli Sample Buffer | Bio-Rad | Cat#1610747 |
| Bodipy 493/503 | Thermo Fisher Scientific | Cat#D3922 |
| Hoechst | Thermo Fisher Scientific | Cat#34580 |
| CyQUANT | Thermo Fisher Scientific | Cat#C7026 |
| 2-deoxy-D-[1- ³ H]-glucose | PerkinElmer | Cat#NET328250UC |
| D-[3- ³ H]-glucose | PerkinElmer | Cat#NET331C001MC |
| Glucose Solution | Thermo Fisher Scientific | Cat#A2494001 |
| Optipase Hisafe 3 | PerkinElmer | Cat#1200.437 |
| Pierce 16% Formaldehyde (w/v), Methanol-Free | Thermo Fisher Scientific | Cat#28906 |
| PF-739 | Aobious | Cat#AOB33584 |
| MK-2206 2-HCl | SellekChem | Cat#S1078 |
| 2-deoxy glucose | Sigma-Aldrich | Cat#D3179-1G |
| Rapamycin | Sigma-Aldrich | Cat#R8781-200UL |
| Precision Plus Protein Blue-Stained Protein Standards 10-250kDa | Bio-Rad | Cat#1610373 |
| Agarose, LE, Analytical Grade | Promega | Cat#V3121 |
| SYBR safe DNA Gel Stain | Thermo Fisher Scientific | Cat#S33102 |
| Complete, EDTA-free Protease Inhibitor Cocktail, Tablets in glass vials | Sigma-Aldrich | Cat#5056489001 |

(Continued on next page)

Continued

| REAGENT or RESOURCE | SOURCE | IDENTIFIER |
|--|--|-----------------|
| PhosSTOP | Sigma-Aldrich | Cat#4906837001 |
| QIAzol lysis reagent | Qiagen | Cat#79306 |
| Creatine phosphate | Roche | Cat#10621714001 |
| Dynabeads Protein G for immunoprecipitation | Thermo Fisher Scientific | Cat#10004D |
| Dynabeads Protein A for immunoprecipitation | Thermo Fisher Scientific | Cat#10002D |
| Q5 Hot Start High-Fidelity DNA Polymerase | New England Biolabs (NEB) | Cat#M0493L |
| Agarose, LE, Analytical Grade | Promega | Cat#V3121 |
| SYBR safe DNA Gel Stain | Thermo Fisher Scientific | Cat#S33102 |
| N1-Methylpseudo-UTP | Saveen Werner | Cat#NU-890L |
| Seahorse XF 100 mm pyruvate solution | Agilent Technologies | Cat#103578-100 |
| Seahorse XF 200 mm glutamine solution | Agilent Technologies | Cat#103579-100 |
| Seahorse XF 1.0 M glucose solution | Agilent Technologies | Cat#103577-100 |
| Seahorse XF DMEM Medium pH 7.4 | Agilent Technologies | Cat#103575-100 |
| Seahorse XF Calibrant Medium pH 7.4 | Agilent Technologies | Cat#100840-000 |
| Plasmids | | |
| HiFi dCas9 VPR | AddGene | Cat#188510 |
| sgRNA | | |
| ID | Sequences | Source |
| CKB knock out | GTGGCTGTTGGAGAAGGGCA | Thermo Fischer |
| CKB CRISPRa 1 | GCTGCGCGGGGTCCCAGCGA | Thermo Fischer |
| CKB CRISPRa 1 | GGCCTCTGGGCGGGAAACTG | Thermo Fischer |
| CKB CRISPRa 1 | GCAGAGGCAAGGGCGTGCGA | Thermo Fischer |
| Primers for <i>in vitro</i> transcription (IVT) | | |
| T7-CKB mRNA Fwd | ACACTAATACGACTCACTATAGGG GCCACCGTTTCGCTGCGTCTCC | Sigma Aldrich |
| T7-CKB mRNA Rev | CAGACGCAGGCAGGCCAAAACCT AGTTTATTTTCAGCATCAGCAGTATCT | Sigma Aldrich |
| T7-dCas9-VPR Fw2 | ATATTTCTAATACGACTCACTATAG CTTTTCGCAACGGGTTTGC | Sigma Aldrich |
| T7-dCas9-VPR Rv2 | AACGAAGCTGTTAAACAGAGATG TGTCGAAGATGGAC | Sigma Aldrich |
| Softwares and Algorithms | | |
| GraphPad Prism | v.10.6.0 | N/A |
| R Studio | v.4.1.1 | N/A |
| ImageJ | v.2.0.0 | N/A |
| Deposited data | | |
| Raw and analyzed data | This paper | GEO: GSE307820 |
| qPCR primers | | |
| Fwd CKB | TCATCCAGACAGGCGTGGAC | Sigma Aldrich |
| Rev CKB | GCTCATCGCTGGGCTTGTAG | Sigma Aldrich |
| Fwd CKMT2 | AGGTGACACCCAACGGCTA | Sigma Aldrich |
| Rev CKMT2 | TGACGGGGTCAAAAAGGTCAG | Sigma Aldrich |
| Fwd HPRT1 | CCTGGCGTCGTGATTAGTGAT | Sigma Aldrich |
| Rev HPRT1 | AGACGTTTCAGTCTGTCCATAA | Sigma Aldrich |
| Fwd B2M | AAGGACTGGTCTTTCTATCTC | Sigma Aldrich |
| Rev B2M | GATCCCACTTAACATCTTGG | Sigma Aldrich |
| Fwd FASN | AAGGACCTGTCTAGGTTTGATGC | Sigma Aldrich |
| Rev FASN | TGGCTTCATAGGTGACTTCCA | Sigma Aldrich |
| Fwd SCD | TTCTACCTGCAAGTTCTACACC | Sigma Aldrich |

(Continued on next page)

Continued

| REAGENT or RESOURCE | SOURCE | IDENTIFIER |
|---------------------|-------------------------|---------------|
| <i>Rev SCD</i> | CCGAGCTTTGTAAGAGCGGT | Sigma Aldrich |
| <i>Fwd ACLY</i> | ATCGGTTCAAGTATGCTCGGG | Sigma Aldrich |
| <i>Rev ACLY</i> | GACCAAGTTTCCACGACGTT | Sigma Aldrich |
| <i>Fwd CD36</i> | CTTTGGCTTAATGAGACTGGGAC | Sigma Aldrich |
| <i>Rev CD36</i> | GCAACAAACATCACCACACCA | Sigma Aldrich |
| <i>Fwd ACACA</i> | ATGCTGGCTTGACCTAGTA | Sigma Aldrich |
| <i>Rev ACACA</i> | CCCCAAAGCGAGTAACAAATTCT | Sigma Aldrich |
| <i>Fwd SLC2A4</i> | TGGGCGGCATGATTTCCTC | Sigma Aldrich |
| <i>Rev SLC2A4</i> | GCCAGGACATTGTTGACCAG | Sigma Aldrich |
| <i>Fwd PPARG</i> | TCATAATGCCATCAGGTTTG | Sigma Aldrich |
| <i>Rev PPARG</i> | CTGGTCGATATCACTGGAG | Sigma Aldrich |
| <i>Fwd CEBPA</i> | AGCCTTGTGTTGACTGTATG | Sigma Aldrich |
| <i>Rev CEBPA</i> | AAAATGGTGGTTTAGCAGAG | Sigma Aldrich |
| <i>Fwd PLIN1</i> | TGGAGACTGAGGAGAACAAG | Sigma Aldrich |
| <i>Rev PLIN1</i> | ATGTCACAGCCGAGATGG | Sigma Aldrich |
| <i>Fwd LPL</i> | TCATTCGCGAGTAGCAGAGT | Sigma Aldrich |
| <i>Rev LPL</i> | GGCCACAAGTTTGGCACC | Sigma Aldrich |
| <i>Fwd ADIPOQ</i> | GGTCTCGAACTCCTGGCCTAA | Sigma Aldrich |
| <i>Rev ADIPOQ</i> | TGAGATATCGACTGGGCATGGT | Sigma Aldrich |
| <i>Fwd FABP4</i> | ACTGGGCCAGGAATTTGACG | Sigma Aldrich |
| <i>Rev FABP4</i> | CTCGTGGAAGTGACGCCTT | Sigma Aldrich |
| <i>Fwd Fasn</i> | GGAGGTGGTGATAGCCGGTAT | Sigma Aldrich |
| <i>Rev Fasn</i> | TGGGTAATCCATAGAGCCCAG | Sigma Aldrich |
| <i>Fwd Scd</i> | TTCTTGCGATACACTCTGGTGC | Sigma Aldrich |
| <i>Rev Scd</i> | CGGGATTGAATGTTCTTGTCGT | Sigma Aldrich |
| <i>Fwd Acly</i> | ACCCTTTCACTGGGGATCACA | Sigma Aldrich |
| <i>Rev Acly</i> | GACAGGGATCAGGATTTCTTG | Sigma Aldrich |
| <i>Fwd Cd36</i> | ATGGGCTGTGATCGGAACTG | Sigma Aldrich |
| <i>Rev Cd36</i> | TTTGCCACGTCATCTGGGTTT | Sigma Aldrich |
| <i>Fwd Acaca</i> | CTCCCGATTGATAATTGGGTCTG | Sigma Aldrich |
| <i>Rev Acaca</i> | TCGACCTTGTTTACTAGGTGC | Sigma Aldrich |
| <i>Fwd Slc2a4</i> | ACACTGGTCCTAGCTGTATTCT | Sigma Aldrich |
| <i>Rev Slc2a4</i> | CCAGCCACGTTGCATTGTA | Sigma Aldrich |
| <i>Fwd Pparg</i> | CTCCAAGAATACCAAAGTGCGA | Sigma Aldrich |
| <i>Rev Pparg</i> | GCCTGATGCTTTATCCCCACA | Sigma Aldrich |
| <i>Fwd Cebpa</i> | CAAGAACAGCAACGAGTACCG | Sigma Aldrich |
| <i>Rev Cebpa</i> | GTCAGTGGTCAACTCCAGCAC | Sigma Aldrich |
| <i>Fwd Fabp4</i> | AAGGTGAAGAGCATCATAACCCT | Sigma Aldrich |
| <i>Rev Fabp4</i> | TCACGCCTTTCATAACACATTCC | Sigma Aldrich |
| <i>Fwd Plin1</i> | CTGTGTGCAATGCCTATGAGA | Sigma Aldrich |
| <i>Rev Plin1</i> | CTGGAGGGTATTGAAGAGCCG | Sigma Aldrich |
| <i>Fwd Adipoq</i> | TGTTCTCTTAATCCTGCCCA | Sigma Aldrich |
| <i>Rev Adipoq</i> | CCAACCTGCACAAGTTCCCTT | Sigma Aldrich |
| <i>Fwd Ckb</i> | AAGTTCTCGGAGGTGCTCAA | Sigma Aldrich |
| <i>Rev Ckb</i> | CCGTTGCTCCATCTCAATG | Sigma Aldrich |
| <i>Fwd Hprt</i> | TCAGTCAACGGGGGACATAAA | Sigma Aldrich |
| <i>Rev Hprt</i> | GGGGCTGTACTGCTTAACCAG | Sigma Aldrich |

(Continued on next page)

Continued

| REAGENT or RESOURCE | SOURCE | IDENTIFIER |
|---------------------|-------------------------|---------------|
| Fwd Lrp10 | GGATCACTTTCCACGTTCTG | Sigma Aldrich |
| Rev Lrp10 | GAGTGCAGGATTAAATGCTCTGA | Sigma Aldrich |
| Fwd Elov3 | TACATCTGGAGGCAGGAGAA | Sigma Aldrich |
| Rev Elov3 | GGTGAAGAAGTGAGCGAATAG | Sigma Aldrich |

EXPERIMENTAL MODEL AND SUBJECT DETAILS

Subjects

Human adipose tissue biopsy data were previously characterized and kindly provided by Prof. Mikael Rydén and Dr. Niklas Mejhert (Karolinska Institutet, Stockholm, Sweden), as described in clinical cohort ^{26,35} and spatial transcriptomics cohorts.³³ All studies were approved by the Regional Board of Ethics in Stockholm, as previously published,^{26,32,33,35} and followed the declaration of Helsinki ethical principles for medical research involving human subjects. Written informed consent was obtained from all subjects.

Cell cultures

Human preadipocyte culture

In vitro differentiated human adipocytes were differentiated from CD55⁺ progenitors and cultured and according to the methodology described in a previous work of our lab.²⁶ In brief, progenitors were isolated from abdominal subcutaneous WAT of one male and one female donor²⁶ and maintained in DMEM containing 10% FBS, 10 mM HEPES, 50 µg/mL penicillin-streptomycin, and 2.5 ng/mL fibroblast growth factor 2 (FGF). At ~90% confluency, FGF was removed, cells were washed with PBS (pH 7.4), and differentiation was induced for 10 days using an adipogenic cocktail.¹² During differentiation, cells were treated with: phosphocreatine (1–30 mM, 24 h), 2-deoxy-D-glucose (0.1 mM, 48 h), rapamycin (500 nM, 48 h), PF-739 (5 µM, 48 h), or MK-2206 (10 µM, 48 h). Low-BCAA medium was generated by replacing DMEM (BCAA 304 mg/L) with F12 medium (BCAA 28.8 mg/L) from day 8 of differentiation for 48 h.

Isolated human primary adipocytes from a male and a female donor were used for cell culture, for transcriptomic analyses,^{26–28} and for proteomics.³¹ All studies were approved by the Regional Board of Ethics in Stockholm, as previously published,^{26–28,31} and followed the declaration of Helsinki ethical principles for medical research involving human subjects. Written informed consent was obtained from both subjects.

Human multipotent adipose-derived stem culture

hMADS cells were maintained in low-glucose DMEM supplemented with 10% FBS, 2 mM L-glutamine, 10 mM HEPES, 50 U/mL penicillin, 50 µg/mL streptomycin, and 2.5 ng/mL human FGF2. Cells were seeded in 6-well plates at 44,000 cells/mL and incubated at 37°C in 5% CO₂. Six days after seeding, FGF2 was removed. On the following day (day 0), differentiation was initiated in serum-free proliferation medium/Ham's F-12 containing 10 µg/mL transferrin, 5 µg/mL insulin, 0.2 nM triiodothyronine, 100 µM 3-isobutyl-1-methylxanthine, 1 µM dexamethasone, and 100 nM rosiglitazone. At day 3, dexamethasone and 3-isobutyl-1-methylxanthine were omitted from the medium, and at day 9, rosiglitazone was also removed. hMADS were generously provided by Prof. Ez-Zoubir Amri (Université Côte d'Azur, Nice, France).

Murine primary adipocyte culture

Primary adipocytes were isolated from inguinal WAT of female mice fed a standard chow diet. Minced adipose tissue was digested in collagenase-containing medium for 1 h at 37°C under lateral shaking (100 rpm). The suspension was filtered through a 100 µm strainer, diluted to 30 mL with PBS, pelleted (10 min, 1,500 rpm), and resuspended in 12 mL DMEM containing 10% fetal calf serum. Cells (0.5 mL/well) were plated in 12-well plates and incubated at 37°C in 95% air/5% CO₂. After 4 h, unattached cells were removed by three PBS washes, and cultures were maintained in fresh medium. After three passages, cells were seeded at 20,000 cells/well in 48-well plates. Differentiation was induced with growth medium containing 2% FBS, 1 µmol/L dexamethasone, 0.5 µmol/L isobutyl-methylxanthine, 100 nmol/L insulin, and 1 µmol/L rosiglitazone for 3 days. Medium was then replaced with growth medium containing 2% FBS and 100 nmol/L insulin for 2 days, followed by growth medium with 2% FBS alone for the final 2–3 days of differentiation.

Animal experiments were performed according to procedures approved by the local ethic committee and received permission from the French “*Ministère de l'Enseignement Supérieur, de la Recherche et de l'Innovation*”. All animal procedures were reviewed and approved by local and national committees and conducted in accordance with the Guide for the Care and Use of Laboratory Animals published by the European Commission Directive 86/609/EEC.

Animals

The generation, housing and diet intervention of mice *Ckb*^{Adipo-Cre} and *Ckb*^{fl/fl} animals has been previously described.²² Male mice were fed a high fat diet for 6 weeks. WAT was obtained from the epididymal WAT and inguinal WAT depots. Samples for qPCR

analyses were snap-frozen in liquid nitrogen immediately. One part of the fresh tissue samples was fixed in 4% formalin (pH 7.0) and used for immunofluorescence analyses as described below. Samples from these animals were generously provided by Dr. Lawrence Kazak (McGill, Montreal, Canada).

Animal experiments were performed according to procedures approved by the Animal Resource Center at McGill University and complied with guidelines set by the Canadian Council of Animal Care, as previously published.²²

METHOD DETAILS

RNA isolation, cDNA synthesis and real-time qPCR

Total RNA was extracted from cells plated in 48 well plates as described previously.²⁶ The concentration, purity and quality of RNA were measured using both Nanodrop 2000 (Thermo Fisher) and Agilent 2100 Bioanalyzer (Agilent Technologies). Conversion of RNA in cDNA was made using iScript cDNA synthesis kits (BioRad) and concentration adjusted at 1 ng/μL. Expression of mRNA levels by qPCR were then measured using Sybergreen master mix assay, Ct values were then used to calculate relative expression with the comparative Ct-method, i.e., $2^{\Delta\text{Ct-target gene}/2^{\Delta\text{Ct-reference gene}}}$. Primer sequences (mice and human) are listed in the key resources table.

In vitro transcription and mRNA-based re-expression

CKB and Catalytically inactive Cas9 fused with tripartite VPR (dCas9-VPR) mRNA were generated using T7-containing primers, amplifying the coding sequence contained in cDNA from cells and plasmid vector respectively. Synthesis of mRNA was then performed using HiScribe T7 ARCA mRNA Kit (with tailing) per manufacturer's instructions. To improve stability, N1-Methylpseudo-UTP was incorporated into the mRNA as previously described.⁷⁵

CRISPRa for endogenous CKB overexpression

mRNA encoding dCas9-VPR was introduced in the cells one day prior to adipogenesis induction with Neon transfection system as previously reported⁷⁵ along with a pool of 3 guides RNA targeting area surrounding CKB transcription start site as listed in the key resources table. Neon transfection conditions utilized to introduce mRNA were the following (1700 V, 20 ms, one pulse).

RNAi and re-expression experiments at D3 and D8

For depletion experiments, siRNA oligonucleotides (final concentration of 20 nM) targeting *CKB*, *MLXIPL* or a non-silencing control were introduced to the cells by electroporation (1,300 V, 20 ms, 2 pulses) using the Neon Transfection system, 100 μL Kit (Invitrogen) at D3 or D8 of differentiation as previously described.²⁶ For re-expression experiments (see above), mRNA encoding *CKB* (20 pmol) or a non-coding control was introduced in the same manner by the Neon Transfection system, 100 μL Kit, (1,300 V, 20 ms, 2 pulses). Cells were then seeded in plates and incubated with the differentiation medium containing adipogenic cocktail until full differentiation. The gene silencing references are listed in the key resources table.

Early transfection of pre-adipocytes (D-1) and incubations with chemicals

Early transfection of pre-adipocytes was performed one day prior to beginning of differentiation. Transfection media was prepared using Pure DMEM Medium, siRNA (non-targeting control, *CKB*, *CKMT2*, 40 nM final concentration) and Dharmafect 3. Hence, the mixture was plated and incubated at room temperature for 30 min before adding cells resuspended in proliferation media at a concentration of 250 cells/μL without FGF. After 24 h cells were washed once with 1x PBS and differentiation cocktail added on cells. When required, cells were trypsinized at day 8 (D8) and transfected again with siRNA targeting *MLXIPL*, *CKB*, or non-silencing control as described above. At day 10 (D10), cells were treated with the indicated chemical compounds.

Library preparation and RNA sequencing

In brief, 100 ng of isolated total RNA from siC, siCKB and siCKMT2 cells were used for library preparation. The quality and yield of the samples were assessed using Qubit (Thermo Fisher) and Tape station (Agilent), thereafter normalized and combined. These pools were sequenced on the Illumina Nextseq 2000 p2 100 cycles sequencing run, generating 59 base single ends read with dual index. Base scaling and demultiplexing was performed using CASAVA software with default settings generating Fastq files aligned to GRCh38 for further downstream mapping and analysis. Raw counts were normalized and analyzed using DESeq2 in R studio (v4.1.1). Pathway analyses were performed using KEGG Human 2021 annotations. Plotting of omics data was performed with ggplot2 and gggraph. The data is deposited in GEO under the accession GEO number GSE307820.

Western Blot analysis

Western blotting was performed as previously described.²⁶ All antibodies are listed in the key resources table. For protein of interest located at the same size, lysates were subdivided in equal amounts and loaded on separate gels.

Immunoprecipitation from whole lysate

Adipocytes were seeded and differentiated in 15 cm² dishes. At D10 post-induction, cells were washed three times in ice-cold PBS followed by one wash with immunoprecipitation (IP) base buffer (10 mM Tris-HCl, pH 7.5; 150 mM NaCl; 0.5 mM EDTA). Cells were

then lysed in 400 μ L of IP lysis buffer (base buffer supplemented with 0.5% NP-40, protease inhibitor cocktail, and phosphatase inhibitor) and collected into 1.5 mL Eppendorf tubes. Lysates were incubated on ice for 30 min with gentle resuspension every 10 min. Following lysis, samples were centrifuged at $17,000\times g$ for 20 min at 4°C. The resulting supernatant was carefully transferred to a new tube, avoiding both the pellet and upper lipid layer, and diluted with 600 μ L of dilution buffer (base buffer supplemented with protease and phosphatase inhibitors).

An aliquot of 100 μ L was removed and stored as input control for subsequent western blot analysis. The remaining lysate was incubated overnight at 4°C on a rotating platform with 3 μ g of antibody (AKT or control IgG). The following day, protein A and G magnetic beads were calibrated separately for 15 min and then combined (30 μ L each per reaction). Beads were added to the antibody-incubated lysates and rotated for an additional 3 h at 4°C to ensure binding.

After incubation, the depleted supernatant was collected and stored. Beads were washed five times in wash buffer (base buffer containing 0.05% NP-40, protease and phosphatase inhibitors), followed by a final wash in ice-cold PBS. Proteins were eluted by resuspending beads in 30 μ L of elution buffer (22.5 μ L RIPA, 7.5 μ L 4x Laemmli sample buffer, 1 mM DTT, protease and phosphatase inhibitors) and incubated at 95°C for 10 min. Eluted proteins and input controls were resolved by SDS-PAGE for immunoblot analysis.

ATP measurement

Measures of cellular ATP levels were performed in cell lysates per manufacturer's instructions. Per well in a 96-well plate, 10,000 to 15,000 cells were seeded at D-1 after transfection with siRNA directed against control or CKB. The assay was performed at D10 post differentiation with the adipogenic cocktail. Data were normalized by protein levels.

Metabolomic samples preparation and targeted metabolomic measurements

Cells were plated in 15 cm² dishes and differentiated up to day 10. Thereafter, cells were washed in cold PBS twice, then scraped in ice-cold 90% methanol, collected and snap frozen in liquid nitrogen. Metabolites extraction and mass spectrometry analysis were carried out as previously described.^{26,30} Metabolites were profiled at the Swedish Metabolomics Center. The cell extracts were split in 3 parts and analyzed by (i) gas chromatography-mass spectrometry (GC-MS) to target TCA metabolites after derivatization, (ii) hydrophilic interaction liquid chromatography-mass spectrometry (HILIC-MS) to target nucleotides, creatine, and other phosphorylated metabolites after reconstitution of the dried extract in 50 μ L of 50% methanol, and (iii) LC-MS to target amino acids after derivatization of the dried extract with AccQ-Tag reagent. The metabolites were annotated by library matching of their retention index (GC-MS) and retention time (LC-MS) and their exact mass.⁷⁸ Mass spectra and retention index comparison from GC-MS analyses was performed using NIST MS v.2.2 software. Both the Swedish Metabolomics Center's in-house standards libraries and public libraries as NIST (<https://chemdata.nist.gov/>) and MoNA (<https://mona.fiehnlab.ucdavis.edu/>) were used. The ¹³C-labeling was calculated by using an in-house script.

Creatine kinase activity

Creatine kinase activity was measured following the manufacturer's instructions. Briefly, cells were seeded on D-1 at a density of 5×10^6 per well in 6-well plates after transfection with either control siRNA (siC) or CKB-targeting siRNA (siCKB). The assay was performed on day 10 of differentiation. Cells were lysed in 200 μ L homogenization buffer (250 mM sucrose, 1 mM Tris-HCl pH 7.4, 1 mM EDTA pH 8, 2% BSA) and passed through a 23 G needle more than 15 times. Lysates were centrifuged at $20,000 \times g$ for 40 min at 4°C, and the supernatant (cytosolic fraction) was collected. Creatine kinase activity was determined using 10 μ L of the cytosolic fraction, according to the manufacturer's protocol. Total protein concentration was measured for normalization, and background signal from siCKB samples was subtracted from all measurements.

ELISA assays

Adiponectin and lactate quantification in cultured media of cells harvested at D10 were performed according to manufacturer instructions. Data obtained were normalized by RNA concentration per well.

Triglyceride extraction and measurement

In brief, cells seeded in 96-well plates, plated at the density of 15,000 cells/well. At D10 of differentiation, triglyceride extraction was performed by using 5% NP40 and employing the Triglyceride Quantification Colorimetric/Fluorometric Kit, following manufacturer instructions.

Immunofluorescence (IF)

Murine WAT samples were fixed in 4% PFA for 24 h at 4°C, embedded in paraffin, and sectioned at 5 μ m thickness. Sections were stained with hematoxylin and eosin (H&E, Sigma-Aldrich) following standard protocols. For immunofluorescence, sections were incubated overnight at 4°C with either SREBP1 antibody (1:50) or anti-CKB antibody (1:100). Detection was performed using anti-rabbit Alexa Fluor 488 (1:500) for CKB or anti-rabbit Alexa Fluor 647 (1:500) for SREBP1, applied for 1 h at room temperature. Nuclear counterstaining was done with Hoechst (1:500) for 20 min at room temperature. Quantification of SREBP1-positive cells was carried out in ImageJ by measuring SREBP1 signal intensity in 3 randomly selected fields per section at 20 \times magnification using an Axio Observer.Z1 inverted fluorescence microscope (Zeiss) with AxioVision software, normalizing total intensity to Hoechst signal.

Confocal microscopy

Images were acquired using a Nikon multipoint spinning disk confocal inverted microscope, equipped with a Kinetix sCMOS camera (6.5 μm pixel size). Imaging was performed with 10 \times , 20 \times , and 40 \times air objectives to capture a range of magnifications suitable for the experimental setup.

Quantification of lipid accumulation (by Bodipy staining)

Cells cultured in 96-well plates were fixed with 4% paraformaldehyde for 10 min at room temperature. Following fixation, they were washed three times with PBS and then stained for 20 min at room temperature with Hoechst 33342 (2 $\mu\text{g/mL}$, #H3570) and BODIPY 493/503 (0.2 $\mu\text{g/mL}$, #D3922), both supplied by Invitrogen (Thermo Fisher Scientific). After staining, the cells were washed three additional times with PBS. Imaging was carried out using a 10 \times objective on the CellInsight CX5 high-content screening system (Thermo Fisher Scientific), following a previously reported protocol. Quantification of nuclei and lipid droplets was performed using the object and spot detection algorithms provided in the HCS Studio: Cellomics Scan software (v6.6.0, Thermo Fisher Scientific), with border nuclei automatically excluded. The lipid droplet area per cell was calculated by dividing the total lipid droplet area in a well by the number of nuclei in that same well.⁷⁹

Seahorse assays

OCR and ECAR were measured with XF96 Seahorse Extracellular Flux Analyzer (Agilent) using Cell Mito Stress and Cell Glyco Stress Test Kits as previously described²⁶. For Mito Stress Test, cells were incubated in medium supplemented with 1 mM pyruvate, 2 mM glutamine and 10 mM glucose for 1 h. Mito Stress assays were performed by sequential addition of 1.5 μM oligomycin (inhibitor of ATP synthesis), 1.5 μM FCCP and 0.5 μM rotenone/antimycin A (inhibitors of complex I and complex III of the respiratory chain, respectively). For Glyco Stress Test, cells were incubated in medium supplemented with 2 mM glutamine for 1 h. Glyco Stress assays were performed by sequential addition of glucose 100 mM, 1.5 μM oligomycin (inhibitor of ATP synthesis) and 2-DG 500 mM. Immediately after the assay, cells were incubated with CyQUANT Kit reagent and fluorescence was measured for data normalization. Fluorescence was quantified using Varioskan LUX (Thermo Fisher Scientific) according to manufacturer instructions.

Radioactive *de novo* lipogenesis measurement

Cells were sensitized to insulin with 1/20 reduction 48 h prior to experiment, 24 h later insulin was completely removed. The day of the experiment cells were then incubated with media containing ³H-glucose (0.1 μM) with and without insulin (150 nM) for 2 h. Cells were then lysed in 0.1% SDS (in H₂O) and the lysates resuspended in 4 mL toluene overnight. Radioactivity was quantified using a beta counter. A portion of each lysate was reserved for protein quantification to normalize DNL measurements.

Radioactive glucose uptake measurement

Cells were sensitized to insulin with 1/20 reduction 48 h prior to experiment, 24 h later insulin was completely removed. On the day of the experiment cells were then incubated with media containing 2-deoxy-D-[1H³]-glucose (0.5 μM) with and without insulin (150 nM) for 40 min. Cells were then washed twice with cold PBS then lysed in 0.1% SDS/H₂O RIPA buffer and resuspended in Optiphas HiSafe for at least 3 h prior to beta counter measurement. Portion of lysate was used for protein quantification using Pierce BCA Protein determination kit (ThermoFisher) for normalization. The rest of the lysate was transferred to cuvettes containing scintillation fluid and counts per minute was recorded using a Liquid Scintillation Analyser (Tri-Carb 4910 TR, PerkinElmer).

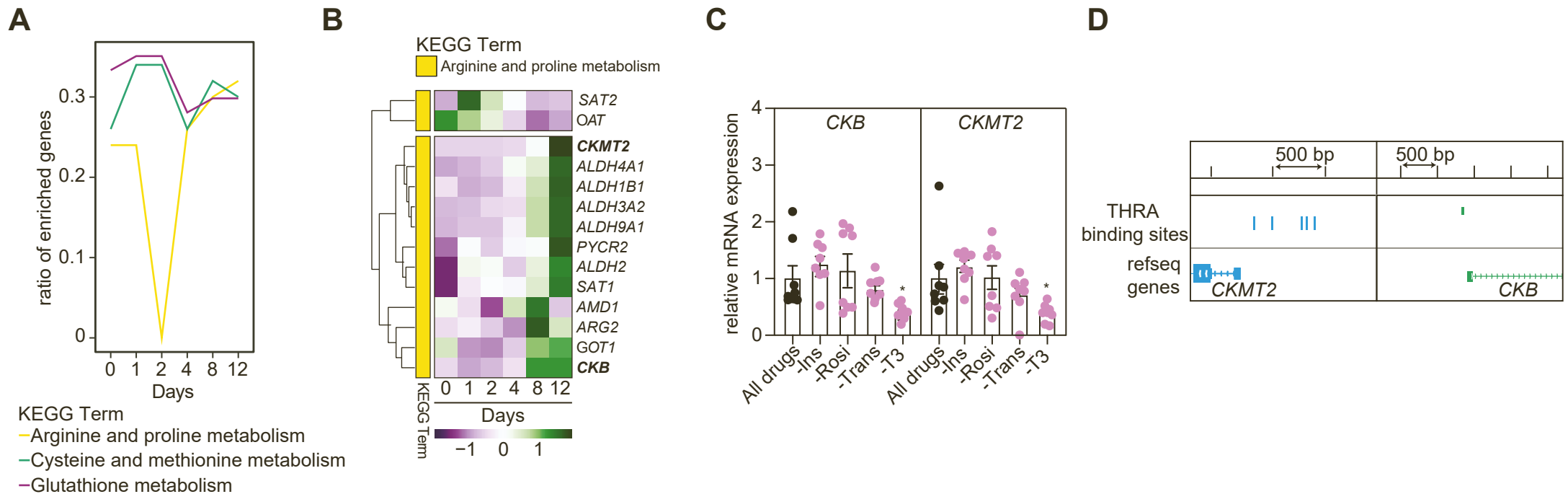
QUANTIFICATION AND STATISTICAL ANALYSIS

Data are reported as mean with SEM unless otherwise stated. Results were compared by Student t-test, One- or Two-way analysis of variance (ANOVA) with Dunnett's or Tukey's post-hoc tests respectively. For correlation analyses in clinical cohorts, simple and multiple regression analyses (with BMI included as independent regressor) were used. Statistical analyses were performed using Prism (GraphPad Software) and bioinformatic analyses using R v.4.1.1.

Supplemental information

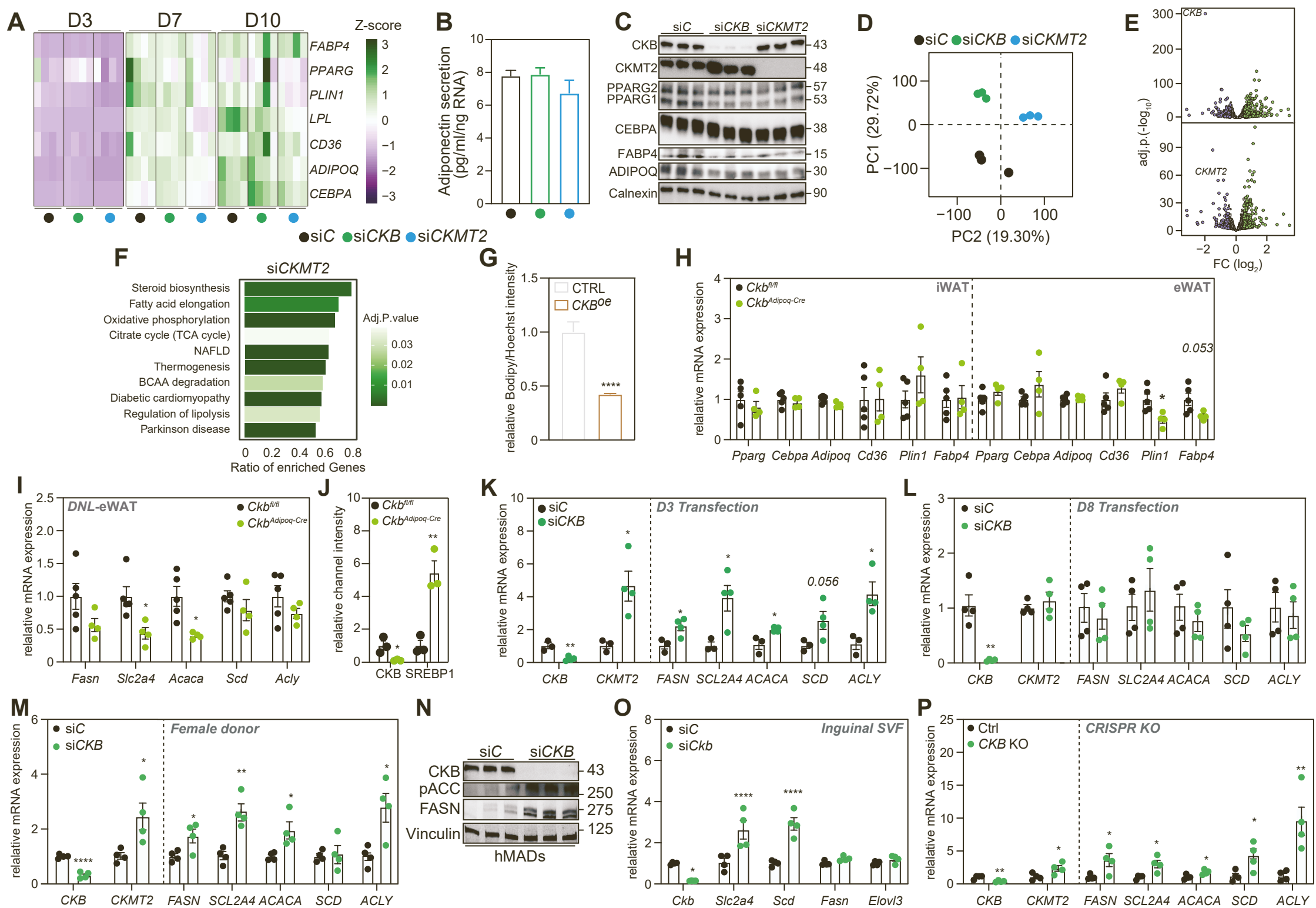
**Creatine kinase B regulates glycolysis and *de novo*
lipogenesis pathways to control lipid
accumulation during adipogenesis**

Gianluca Renzi, Romane Higos, Ivan Vlassakev, Abdoul Akim Bello, Muhmmad Omar-Hmeadi, Mattias Hansen, Fatiha Merabtene, Christine Rouault, Ondrej Hodek, Lucas Massier, Bruno Antonny, Geneviève Marcelin, Janane F. Rahbani, Simon Lecoutre, and Salwan Maqdasy



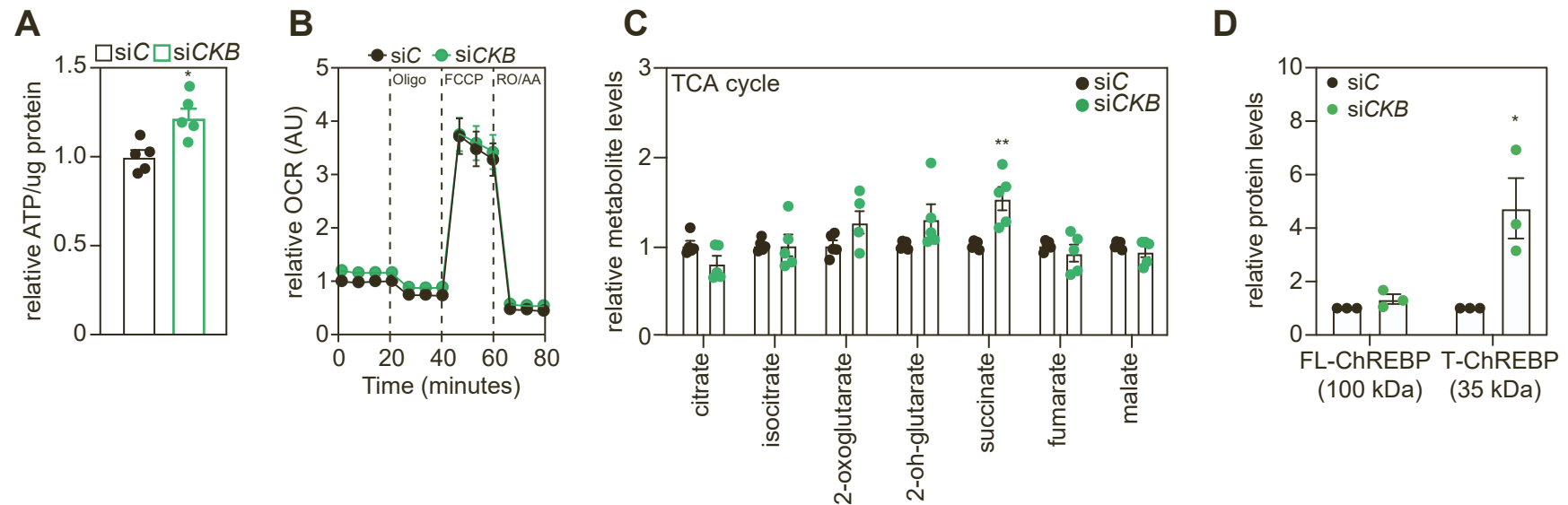
Supplementary Figure 1: Temporal induction of creatine kinases during adipogenesis is driven by thyroid hormone signaling.

- (A) Time course plot, representing trend of enrichment of amino acid related pathways during *in vitro* differentiation of human white preadipocytes from FANTOM5 data²⁷. On the y axis is displayed the enrichment ratio of genes/tot gene ontologies, on the x axis is specified the day of adipocyte differentiation.
- (B) Heatmap representing changes in gene expressions of the genes enriched in “Arginine and proline metabolism” KEGG pathway throughout preadipocyte differentiation.
- (C) mRNA expression of *CKB/CKMT2* in *in vitro* differentiating human white preadipocytes incubated with media lacking one of the components of the adipogenic cocktail from D5 to D8 of differentiation. Values are mean \pm SEM. *p* value was calculated with One-way ANOVA with Dunnett’s multiple-comparison test, * *p* < 0.05 when compared to the “all drugs” condition. Ins = Insulin; Rosi = Rosiglitazone; Trans = Transferrin.
- (D) Graphical visualization of genomic area of Chromosome 14 and Chromosome 5 with focus on *CKB/CKMT2* TSS and 1000 base pairs upstream to it on the first row, annotated thyroid receptor A (THRA) binding sites, on the second row the annotated gene.



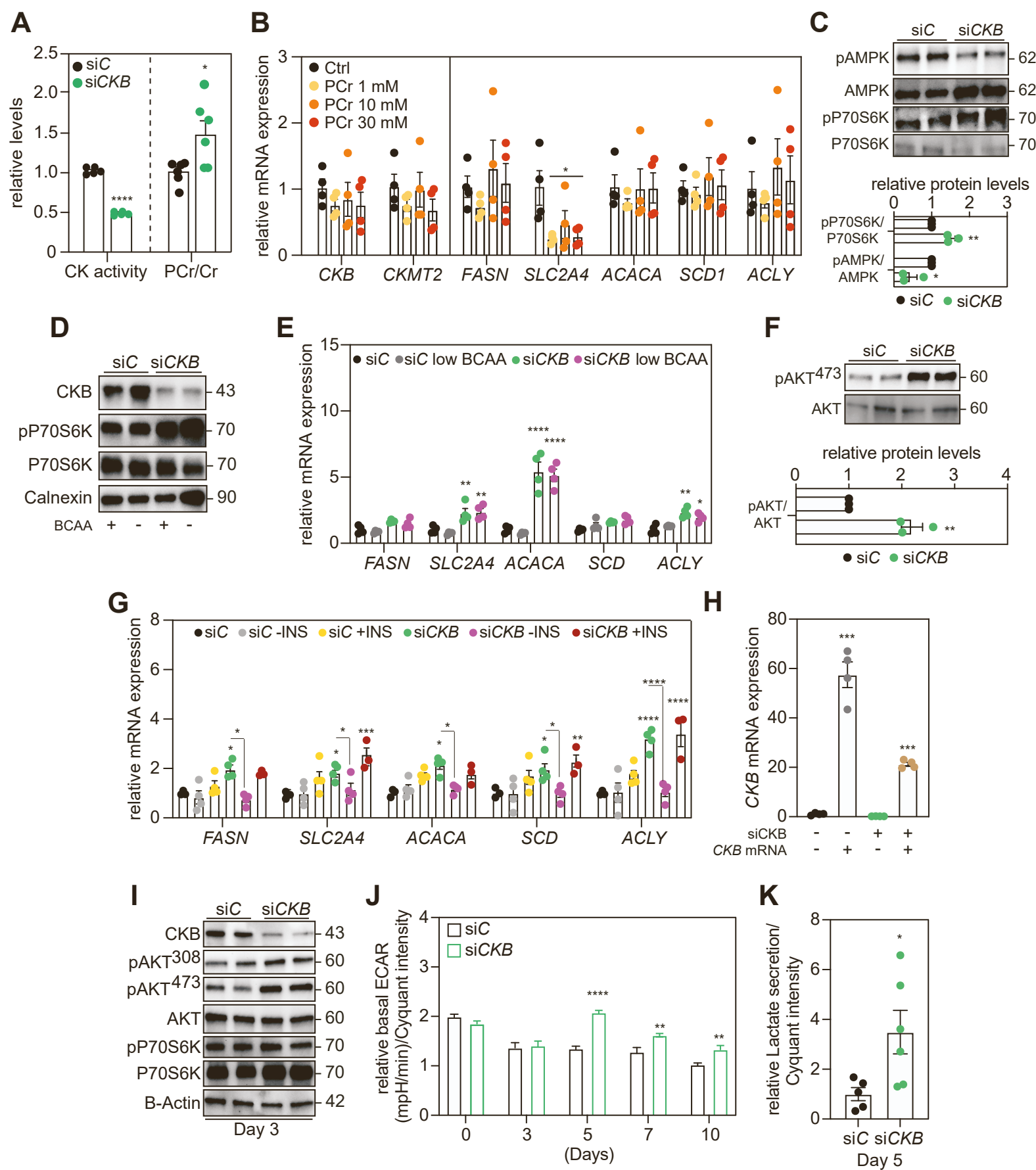
Supplementary Figure 2: Creatine kinase B regulates *de novo* lipogenesis without altering adipogenesis.

- (A) Heatmap representing mRNA expression quantified by qPCR for several markers of mature adipocytes in siC/siCKB/siCKMT2 cells transfected at D-1 and harvested at different days of differentiation (D3/D7/D10). Values are centered and scaled according to row mean.
- (B) Secretion of ADIPOQ in media harvested at D10 from siC/siCKB/siCKMT2 cells transfected with siRNA at preadipocyte level (D-1). Values are mean \pm SEM. $n > 10$.
- (C) Representative immunoblots of multiple mature adipocyte markers in siC/siCKB/siCKMT2 cells transfected at D-1 and harvested at D10 of differentiation.
- (D) Dimension 1 and 2 from principal component analysis of 9 samples, data were generated through RNA sequencing of siC/siCKB/siCKMT2 cells transfected at D-1 and harvested at D10 of adipocyte differentiation for analysis.
- (E) Volcano plots displaying differentially expressed genes of cells transfected with siC/siCKB/siCKMT2 at preadipocyte level and harvested D10 of differentiation for analysis.
- (F) KEGG pathways enriched in siCKMT2 compared to siC, color represents significance of enrichment and on the x axis is displayed the enrichment ratio of genes/tot gene ontologies.
- (G) High-throughput quantification of the immunohistochemical Bodipy staining of cells transfected with mRNA encoding catalytically inactive Cas9 coupled to a VPR complex with/without guide RNA targeting *CKB* promoter, transfected at D-1 and harvested at D10 of differentiation. Values are normalized by Hoechst intensity and represented as mean \pm SEM. $n > 10$, p value was calculated by Student's t-test, **** $p < 0.0001$.
- (H) mRNA expression by qPCR of mature adipocyte markers from inguinal and epididymal WAT of *Ckb^{fl/fl}* and *Ckb^{Adipoq-Cre}* male mice. Values are mean \pm SEM. p value was calculated by Student's t-test, * $p < 0.05$.
- (I) mRNA expression of DNL-related genes in epididymal WAT of *Ckb^{fl/fl}* and *Ckb^{Adipoq-Cre}* male mice. Values are mean \pm SEM. p value was calculated by Student's t-test, * $p < 0.05$.
- (J) Relative immunofluorescence signal quantification normalized over Hoechst intensity of CKB/SREBP1 in paraffin embedded inguinal WAT of *Ckb^{fl/fl}* and *Ckb^{Adipoq-Cre}* male mice. Values are mean \pm SEM. p value was calculated by Student's t-test, * $p < 0.05$, ** $p < 0.01$.
- (K) mRNA expression of *CKB/CKMT2* and DNL-related genes in siC/siCKB preadipocytes transfected at D3 of differentiation, harvested at D10. Values are mean \pm SEM. p value was calculated by Student's t-test, * $p < 0.05$, ** $p < 0.01$.
- (L) mRNA expression of *CKB/CKMT2* and DNL-related genes in siC/siCKB cells transfected at D8 of differentiation, harvested at D10. Values are mean \pm SEM. p value was calculated by Student's t-test, ** $p < 0.01$.
- (M) mRNA expression of *CKB/CKMT2* and DNL-related genes in siC/siCKB early transfected (D-1) preadipocytes derived from a female donor, harvested at D10. Values are mean \pm SEM. p value was calculated by Student's t-test, * $p < 0.05$, ** $p < 0.01$, **** $p < 0.0001$.
- (N) Representative immunoblot of siC/siCKB in hMADs transfected at D-1 and harvested at mature state. It displays the upregulation of multiple DNL-related proteins upon *CKB* knockdown.
- (O) mRNA expression of *Ckb* and DNL-related genes in siC/siCkb early transfected preadipocytes isolated from inguinal WAT of female mice and differentiated *in vitro*. Values are mean \pm SEM. p value was calculated by Student's t-test. * $p < 0.05$, **** $p < 0.0001$.
- (P) mRNA expression of *CKB/CKMT2* and DNL-related genes in siC/siCKB early transfected preadipocytes using CRISPR/Cas9 knockout technology, harvested at D10. Values are mean \pm SEM. p value was calculated by Student's t-test, * $p < 0.05$, ** $p < 0.01$.



Supplementary Figure 3: CKB depletion enhances ATP production without mitochondrial activation.

- (A) ATP levels in siC/siCKB cells transfected at D-1 and harvested at D10 of differentiation. Values are relative, normalized by protein concentration and represented as mean \pm SEM. p value was calculated by Student's t-test, * $p < 0.05$.
- (B) Representative Mito stress test demonstrating oxygen consumption rate (OCR) in siC/siCKB cells transfected at D-1 and analysed at D10 of differentiation. Values are represented as mean \pm SEM. Oligo = Oligomycin; FCCP = Carbonil cianuro-p-trifluorometossifenilidrazone; RO/AA = Rotenone/Antimycin.
- (C) Levels of targeted metabolites involved in the TCA cycle of siC/siCKB cells transfected at D-1 and harvested at D10 of differentiation. Values are mean \pm SEM. p value was calculated by Student's t-test, ** $p < 0.01$.
- (D) Relative protein quantification of ChREBP isoforms in siC/siCKB cells transfected at D-1 and harvested at D10 of differentiation (calculated from two independent experiments). Values are mean \pm SEM. p value was calculated by Student's t-test, * $p < 0.05$. FL = full length; T = transcriptionally active isoform of ChREBP.



Supplementary Figure 4: CKB modulates glycolysis and DNL by regulating AKT phosphorylation.

- (A) On the left, creatine kinase activity of isolated cytosolic fraction at D10 of siC/siCKB cells transfected at D-1. On the right, metabolite levels of phosphocreatine/creatine ratio at D10 of differentiation in siC/siCKB cells. Values are mean \pm SEM. p value was calculated by Student's t-test, $*p < 0.05$, $****p < 0.0001$.
- (B) mRNA expression of *CKB/CKMT2* along with DNL-related genes in *in vitro* differentiated adipocytes incubated with sequential doses of phosphocreatine for 24 hours at D10 of differentiation. Values are mean \pm SEM. p value was calculated with One-way ANOVA and Dunnett's multiple-comparison test comparing to control, $*p < 0.05$.
- (C) Representative immunoblot of siC/siCKB cells transfected at D-1, showcasing AMPK/pAMPK and P70S6K/pP70S6K with relative quantification on the bottom (quantification from two independent experiments). Values are mean \pm SEM. p value was calculated by Student's t-test, $*p < 0.05$, $**p < 0.01$. Please note that these blots are revealed from the same proteins as the blot on Figure 3C, where CKB and a B-Actin are presented.
- (D) Representative immunoblot of siC/siCKB cells transfected at D-1 incubated with media containing normal or low BCAA concentration for 48 hours at D8 and harvested afterward.
- (E) mRNA expression by qPCR of DNL-related genes of siC/siCKB cells transfected at D-1 incubated with media containing normal or low BCAA concentration for 48 hours at D8 and harvested afterward. Values are mean \pm SEM. p value was calculated with Two-way ANOVA and Tukey's multiple-comparison test, comparing all conditions to control, $*p < 0.05$, $**p < 0.01$, $****p < 0.0001$.
- (F) Representative immunoblot of siC/siCKB cells, showcasing pAKT/AKT with relative quantification on the bottom (quantified from two independent experiments). Values are mean \pm SEM. p value was calculated by Student's t-test, $**p < 0.01$. Please note that these blots are revealed from the same proteins as the blot on Figure 3C, where CKB and a B-Actin are presented.
- (G) Representative DNL-gene expression by qPCR of siC/siCKB cells transfected at D-1. At D10, cells were starved from insulin for 48 hours (-INS) and consequently stimulated for 2 hours with insulin (+INS), post-starvation. Values are mean \pm SEM. p value was calculated with Two-way ANOVA and Tukey's multiple-comparison test comparing to siC unless indicated otherwise, $*p < 0.05$, $**p < 0.01$, $***p < 0.001$, $****p < 0.0001$.
- (H) mRNA expression by qPCR of *CKB* of early transfected (at D-1) siC/siCKB cells, re-transfected at D8 with mRNA encoding *CKB* or a non-coding sequence. Values are mean \pm SEM. p value was calculated with Two-way ANOVA and Tukey's multiple-comparison test comparing to siC, $***p < 0.001$.
- (I) Representative immunoblot of early siC/siCKB transfected cells (D-1) harvested at D3 of adipocyte differentiation.
- (J) Representative basal ECAR of Seahorse (Glycostress) analysis during preadipocyte differentiation in siC/siCKB cells transfected at D-1. The analyses were performed on different days of differentiation (from D0 to D10). Values are mean \pm SEM. p value was calculated by a Student's t-test for each day. $n > 10$, $**p < 0.01$, $****p < 0.0001$.
- (K) Lactate secretion in siC/siCKB cells transfected at D-1, measured at D5 of differentiation. Values are mean \pm SEM and normalized by Cyquant intensity. p value was calculated by Student's t-test, $*p < 0.05$.